GeoResearch Forum Vols. 3-4 (1998) pp. 17-54

Global Glacial Isostasy and Relative Sea Level: Implications for Solid Earth Geophysics and Climate System Dynamics

W.R. Peltier

Department of Physics, University of Toronto, Toronto, Ontario M5S 1A7, Canada
E-Mail: peltier@atmosp.physics.utoronto.ca

Keywords: Mantle Viscosity, Inverse Theory, Glacial Rebound, Ice-Ages

Abstract. The global theory of the glacial isostatic adjustment (GIA) process that has been developed at Toronto over the past two decades has delivered, and continues to deliver, important new insights into the physics of the planetary interior and into the nature of the climate variability that has occurred on its surface since mid-Pleistocene time. The 100,000 year quasi-periodic ice-age cycle, that has been the dominant feature of this variability, is associated with such large exchanges of mass between the oceans and the continental ice-sheets that the response of the planet to the changing surface load has come to be indelibly recorded in the geological record. Taken together with the geophysical and astronomical signatures of this process, the geological data may be formally inverted to recover detailed information on both the viscosity of the planetary interior and on the variations of ice-sheet thickness that have occurred on its surface. The basic structure of the global viscoelastic theory of the glacial isostatic adjustment process is reviewed herein and several applications are described in order to illustrate the range of its applicability. These illustrations include the inverse problem for mantle viscosity, the prediction of three dimensional crustal motions due to the GIA process that are now being measured using space-geodetic techniques, the inference of ice-sheet thickness variations since last glacial maximum and finally the feedback of the GIA process onto the ice-age cycle itself.

1. Introduction

The origins of the modern global viscoelastic theory of the glacial isostatic adjustment process may be traced to a series of papers that were written in the mid-1970's. The key mathematical result was described in [1] wherein a method was developed whereby the impulse response (Green) functions could be constructed that are required to compute the visco-elastic response of the planet to an arbitrary variation of surface mass load. In the case that the rheology of the mantle could be described as a linear viscoelastic Maxwell solid, it was therein shown that the formalism described in [2] for the elastic problem could be simply extended by invoking the Correspondence Principle of viscoelasticity (e.g. [3]). Application of this method led to the determination of a set of time-dependent Love numbers (h, k ℓ) in terms of which any signature of the viscoelastic response of the planet to a surface mass load could be represented. In [4] it was subsequently demonstrated that the time dependence of these Love numbers (named for A.E.S. Love, e.g. [5], who first employed them to describe the elastostatic case in which the "load" was that associated with the variations of the gravity field responsible for the solid-earth tides) could

be represented using a "viscoelastic normal-mode formalism". In this early analysis the amplitudes of the modes of pure exponential decay were determined using the same collocation technique as had been introduced in [1]. This was later replaced in [6] by the more conventional residue theory representation that had been briefly tested for simple models in [7]. There continues to be some sporadic discussion in the literature as to whether and under what circumstances this discrete spectral representation of the impulse response may be incomplete [8]. There are in fact a limited set of circumstances in which a true continuous spectrum may exist, and even circumstances in which the normal mode "poles" have complex inverse relaxation time, but these circumstances seem not to be physically relevant for the most part and I will have no further need to comment upon them in what is to follow. More important is the fact that in the spectral representation of the ℓ Love number [9] one is obliged to retain the contributions to the discrete spectrum from the dense set of modes that cluster near the Maxwell time(s) of the medium [10] and which I therefore continue to refer to as "transition" modes. For elastically compressible Earth models, this dense set of modes (essentially an infinite set) approximates a continuous spectrum. Examples of the inverse relaxation time and amplitude spectra, in terms of which these viscoelastic surface load Love numbers are represented, will be provided in the following Section of this paper.

Although these aspects of the viscoelastic field theory in terms of which the global GIA process is described are in themselves interesting from a technical perspective, the formalism in which the impulse response functions are employed actually involves much more than the computation of simple space-time convolutions of these impulse response functions with an appropriate assumed history of surface loading. Arguing by analogy with the problem of incorporating the "feedback" of the elastic yielding of the sea floor under the ocean tides onto the tides themselves (see [11]), Farrell and Clark [12], using the results of Peltier ([1], [10]) and [13]), developed a primitive form of a "Sea Level Equation" with which an accurate global model of the variations of relative sea level that occur due to ice-sheet melting might be provided. This integral equation, like that which appears in the above mentioned theory of the ocean tides, is a construct of first order perturbation theory, the solution of which answers the question as to where in the oceans the meltwater produced by ice-sheet disintegration must be put in order that mean sea level (msl) remain a surface of constant gravitational potential (the geoid of classical geodesy). Initial solutions of this integral sea level equation, based upon the simple ICE-1 deglaciation model of [13], were presented in Clark, Farrell and Peltier [14] and Peltier, Farrell and Clark [15]. Even though the ICE-1 model of [13] was extremely primitive, for example it contained no Antarctic component in the deglaciation history, these solutions of the Sea Level Equation immediately provided an explanation of one aspect of postglacial relative sea level (rsl) history that had never previously been explained. This was the observation based upon rsl data from islands in the equatorial Pacific Ocean that sea levels fell continuously from about 5000 years ago when a high stand was recorded that is now approximately 2 m above present sea level.

In the two decades that have passed since this gravitationally self consistent theory of the GIA process was first described, many geophysical, geological and astronomical observations other than postglacial relative sea level histories have also been shown to be explicable (or inexplicable!) in terms of the same theoretical structure. For example initial attempts in [16] and [17] to explain the observed free air gravity anomaly over the Hudson Bay region eventually led to the recognition

[18] that this signal could not be explained as a consequence of incomplete postglacial rebound of the crust but rather was almost entirely a consequence of the mantle convection process (see [19] for a detailed demonstration of this fact). An equally important additional data type that has been fully incorporated into the GIA lexicon consists of observations of certain anomalies in Earth rotation, specifically the so-called non-tidal acceleration of rotation which causes the length of day to increase more slowly than it would under the action of tidal friction alone, and the true wander of the north pole of rotation with respect to the surface geography that is presently occurring at a rate near 0.95 degrees per million years, southwards and along the 76° West meridian [20]. Initial analysis in [21], later corrected in [22] and [23], demonstrated that both of these observations were also explicable entirely in terms of the GIA process when the model of the radial variation of mantle viscosity was fixed to that required to fit postglacial rsl histories from regions that were once ice-covered.

One of the most exciting developments in this area of research in the very recent past, and one that continues to provide great scientific opportunity at present, has involved the impact that space geodetic techniques are having upon the observational definition of GIA related effects. The first such observation was of the non-tidal acceleration of rotation based upon the use of laser ranging observations of the LAser GEOdynamics Satellite (LAGEOS). This observation was first reported in [24] and had been anticipated in [22] and was fully explained in terms of the modern theory of the GIA process in [25]. The second observation of another aspect of the GIA process based upon space geodesy was much more recent and involved the demonstration [26] that the radio-telescopes employed in the network used for Very Long Baseline Interferometry and located near regions that were glaciated at last glacial maximum were clearly observing the present day vertical motion associated with the GIA process. This analysis was based upon the original data reduction of Jim Ryan and Chopo Ma of the Goddard Space Flight Center and involved a comparison of the VLBI observations with the predictions of the ICE-4G model of [27] as tabulated in [9] for all three components of the crustal motion vector at the locations of each of the individual telescopes. Most recently and in the context of the Fennoscandian BIFROST project [29] the Global Position System (GPS) technique has been employed to observe the horizontal motions induced by the GIA process in the region surrounding the Gulf of Bothnia. The slight extension of theory required to predict this aspect of the GIA process has been discussed in [30], [31] and [9]. As I will discuss in what follows, it has recently been demonstrated [32] that such observations of horizontal motion may in fact be highly diagnostic of upper mantle viscosity structure.

Although consideration of such solid earth geophysical processes continues to dominate the scientific agenda related to our understanding of the Dynamics of the Ice-Age Earth, it is nevertheless true that the implications of this work for our understanding of climate system history and dynamics have also begun to attract increasing attention. As it happens, GIA observations may be invoked to clarify a number of issues in this area. Perhaps of greatest importance, in this regard, is that rsl data from regions once covered by ice may be employed to "weigh" the ice that must have been removed to induce the observed variations of relative sea level [27]. Knowing this weight (per unit area) one may therefore infer ice thickness and from ice thickness and the "Sea Level Equation" one may infer the time dependence of the topography with respect to sea level

[27], [28]. Since the topography of the solid Earth with respect to sea level is a vital input to the reconstruction of climate state using an atmospheric general circulation model, it will be clear that GIA analyses have a fundamental role to play in this regard. Computations of this time-dependent topography based upon the ICE-4G model ([27], [33]) are currently in use in the context of the Paleoclimate Model Intercomparison Project (PMIP, see [34]). A further issue in climate system history and dynamics on which the GIA process bears concerns the dynamics of the 100,000 year cycle of ice-age recurrence itself. Recently constructed detailed models of this astronomically driven climate oscillation (e.g. see [35], [36], [37] and references therein) demonstrate that the GIA process plays a fundamental role in driving the sharp "terminations" of the epochs of glaciation which are the single most characteristic feature of the ice-age cycle itself. Of equivalent interest from a climate dynamics perspective, though on a much shorter timescale, is the important contribution that the GIA process makes to the secular variations of sea level that are observed on modern tide gauge recordings [38], [39], [40]. These analyses show that the ongoing GIA process significantly contaminates the data on the basis of which the average rate of global sea level rise is estimated, an important fact since it is widely believed that this process is related to the climate warming that has occurred during the last century.

In the body of this article to follow, I will begin in Section 2 by reviewing the Sea Level Equation component of the global theory of the GIA process that is basic to all of the analyses of this process that will be subsequently discussed. For want of space, it will be possible here to present only a representative sample of the most recent and, I believe, most important examples of these analyses. In addressing the implications of this work for the physics of the solid earth in Section 3, I have elected to focus on providing a summary of recent results concerning the inverse problem for mantle viscosity and on a discussion of the compatibility of the results of this work with requirements of the convection theory of continental drift and sea floor spreading. Three dimensional crustal motion predictions will also be presented. In Section 4, I provide a discussion of the implications of the theory of the GIA process for ice-age paleotopography and, because of the strong connectivity, for the ice-age cycle itself. A discussion of the importance of the ongoing GIA process to the understanding of sea level history in the far field of the ice-sheets, including the variations which define the present day average rate of global sea level rise, will be found in [41], [42] and elsewhere in this volume. The interested reader will find a complete review of these ideas in [37].

2. The Sea Level Equation and its Iterative Solution

As mentioned in the Introduction, the cornerstone of the modern theory of the global process of glacial isostatic adjustment is the integral equation that I have previously referred to as the Sea Level Equation. In schematic form this equation may be written:

$$S(\theta,\lambda,t) = C(\theta,\lambda,t)\left[G(\theta,\lambda,t) - R(\theta,\lambda,t)\right] \tag{1}$$

in which S is relative sea level (rsl) at latitude θ, longitude λ and time t. The function $C(\theta, \lambda, t)$ is the so-called ocean function which is by definition unity where there is ocean and zero where there is land or land-locked water. G is the geoid of classical geodesy which is defined by the

surface of constant gravitational potential that is coincident with mean sea level (msl) over the oceans, but which of course has global definition. R is the local radius of the solid earth. Eustatic variations of rsl are those caused by variations of G whereas isostatic variations of rsl are those caused by variations of R. It is a characteristic of the GIA process that S is driven by both causes simultaneously. It is important to recognize that the ocean function C is time dependent in consequence of the fact that coastal regions may be inundated by the sea as the great continental ice sheets melt during deglaciation ("termination") and similarly the land may rise out of the sea in regions that were ice covered due to the postglacial "rebound" of the crust.

In [1], [10], [13] and [6] detailed mathematical analyses were presented which allowed determination of G and R in terms of linear viscoelastic Green functions assuming that the rheology of the mantle of the Earth could be represented by the three dimensional linear Maxwell model. Representing the variation of surface mass load, with its distinct (mass conserving) ice and water components, by L(θ, λ, t), this equation may be written explicitly as:

$$S(\theta,\lambda,t) = C(\theta,\lambda,t)\cdot\left[\int_{-\infty}^{+\infty} dt' \iint_{\Omega} d\Omega\, L(\theta',\lambda',t')\left(\frac{\phi^L(\gamma,t-t')}{g} - \Gamma^L(\gamma,t-t')\right) + \frac{\Delta\Phi(t)}{g}\right] \quad (2)$$

and the composite property of L may be recognized explicitly by writing it in the form:

$$L(\theta,\lambda,t) = \rho_I I(\theta,\lambda,t) + \rho_w S(\theta,\lambda,t)\ , \quad (3)$$

where ρ_I and ρ_w are the densities of ice and water respectively and where I(θ, λ,t) is the history of continental ice sheet thickness variations. Because the rsl history S occurs not only on the left-hand-side of (2) but also in the triple convolution integral on the right-hand-side, it is clear that (2) is an integral equation. As demonstrated in [1], [10] and [6], the viscoelastic impulse response Green functions, ϕ^L and Γ^L for the gravitational potential perturbation and for radial displacement respectively, may be written in the form:

$$\phi^L(\gamma,t) = \frac{ag}{m_e}\sum_{\ell=o}^{\infty}(1+k_\ell^L(t))P_\ell(cos\,\gamma) \quad (4a)$$

$$\Gamma^L(\gamma,g) = \frac{a}{m_e}\sum_{\ell=o}^{\infty}h_\ell^L(t)P_\ell(cos\,\gamma) \quad (4b)$$

In these expressions the superscript L is employed to signify a surface load Love number, "a" is the radius of the Earth, g is the surface gravitational acceleration, m_e is the Earth's mass and the P_ℓ are Legendre polynomials of degree ℓ. These Green functions depend solely upon the angle γ between source-point (θ′, λ′) and field point (θ, λ) because the Earth model has been assumed to be spherically symmetric. The time dependent function ΔΦ(t) in (2) is introduced to ensure that mass is conserved such that exactly the mass produced by melting ice appears in the oceans.

For the linear viscoelastic Maxwell rheology of the mantle, the constitutive relaxation

between stress and strain, in the domain of the Laplace transform variable s in which the Correspondence Principle is applied, is just:

$$\tau_{ij}(s) = \lambda(s)\, e_{ii}\, \delta_{ij} + 2\,\mu(s)\, e_{ij}(s) \tag{5}$$

in which the viscoelastic compliances $\lambda(s)$ and $\mu(s)$ are simply:

$$\lambda(s) = \frac{\lambda_e s + \mu_e\, \kappa/\nu}{s + \mu_e/\nu} \tag{6a}$$

$$\mu(s) = \frac{\mu_e\, s}{s + \mu_e/\nu}\ . \tag{6b}$$

Since the bulk modulus $\kappa = \lambda(s) + 2\mu(s)/3$ is independent of s (frequency), this model clearly has no bulk dissipation. The quantity $T_m = \nu/\mu_e$ in (6) is called the Maxwell time and this is the timescale that must be exceeded in order to effect the transition from Hookean elastic to Newtonian viscous behaviour that is embodied in the Maxwell model. Since the elastic parameters λ_e and μ_e may be inferred on the basis of the observed depth dependent speeds of seismic shear and compression waves, the only free parameter in the Maxwell model is the molecular viscosity $\nu(r)$. In the event that the spectrum of viscoelastic normal modes required to synthesize the time dependent response of the planet to surface load forcing may be approximated as discrete, then it has been shown in [1], [10] and [6] that the surface load Love numbers appearing in (4) may be written:

$$h_\ell^L(t) = h_\ell^{L,E}\,\delta(t) + \sum_{j=1}^{M} r_j^\ell\, e^{-s_j^\ell t} \tag{7a}$$

$$k_\ell^L(t) = k_\ell^{L,E}\,\delta(t) + \sum_{j=1}^{M} q_j^\ell\, e^{-s_j^\ell t} \tag{7b}$$

where the $h_\ell^{L,E}$ and $k_\ell^{L,E}$ are precisely the elastic surface load Love numbers of [2] and where the $(r_j^\ell,\ q_j^\ell,\ s_j^\ell)$ are the amplitudes and inverse relaxation times of the set of M purely exponential decays that are required to specify the time domain behaviour of $h_\ell^L(t)$ and $k_\ell^L(t)$. As first established in [10], the inverse relaxation times s_j^ℓ are determined by the zeros of an appropriate secular function whereas the modal amplitudes may be determined either by collocation as in [1] or using the theory of residues as in [6].

For the purpose of all of the discussion to follow, I will be concerned with one or the other of the three viscosity models labelled VM1, VM2 and VM3 on Figure 1. Relaxation spectra (the set of s_j^ℓ) for each of these models are shown on Figure 2 whereas the amplitude spectra for model VM2 are shown on Figure 3 for each of the h, k and ℓ Love numbers. The ℓ Love number is not required in (2) but it plays a fundamental role in describing the tangential motion associated with the GIA process and may be written:

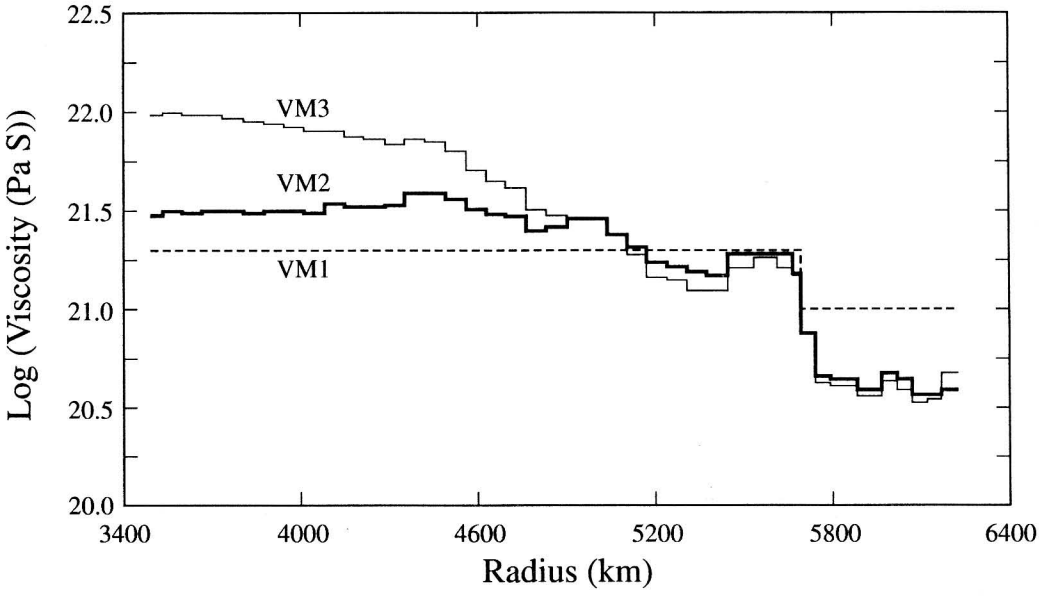

Fig. 1. Illustrates the viscosity models VM1, VM2 and VM3 that are discussed in detail in the later sections of the text.

$$\ell_\ell^L(t) = \ell_\ell^{L,E}\,\delta(t) + \sum_{j=1}^{M} t_j^\ell\, e^{-s_j^\ell t} \tag{7c}$$

It is important to understand that these non-dimensional viscoelastic Love numbers are respectively related to the radial displacement U_ℓ (h), the tangential displacement V_ℓ (ℓ), and to the gravitational potential perturbation Φ_ℓ (k) as:

$$\begin{bmatrix} U_\ell \\ V_\ell \\ \Phi_\ell \end{bmatrix} = \Phi_{2,\ell} \begin{bmatrix} h_\ell^L / g \\ \ell_\ell^L / g \\ k_\ell^L \end{bmatrix} \tag{8}$$

in which $\Phi_{2,\ell}$ is the gravitational potential perturbation of degree ℓ due to the point mass load which is applied to the surface of the planet in determining the impulse response of the system. The full apparatus that is required to specify the integral equation (2) is therefore in place.

This form of the Sea Level Equation is nevertheless somewhat incomplete, at least in principle, because it fails to account for the influence upon rsl history of the modification of the rotational state of the planet that is caused by the redistribution of surface mass load. This additional influence, which as we will show turns out to be small, may be simply accounted for through the use of a modified form of (2) that employs the theory of the viscoelastic rotational response to the changing surface load described in [22] and [23] (a slightly more complete form of this theory was recently presented in [43] and [44]). Now the rotational response to a known

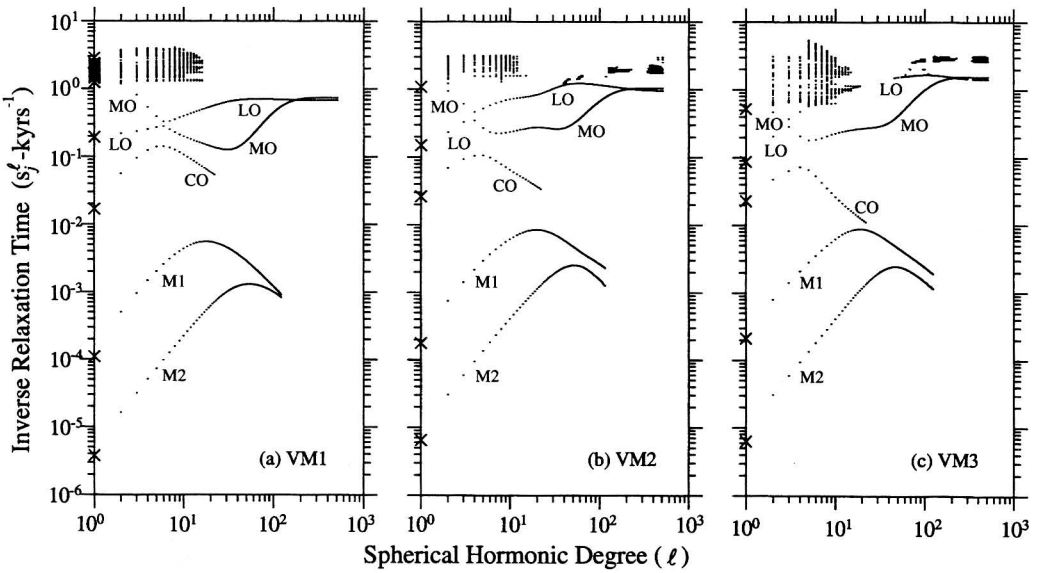

Fig. 2. Relaxation spectra for the spherically symmetric viscosity models VM1, VM2 and VM3. The primary modes of visco-elastic decay are those denoted MO, CO, M1, M2 and LO according to the nomenclature of Peltier (1976). The dense set of modes in the vicinity of $(s_j^\ell)^{-1}$ = 1 kyr are the transition modes identified in Peltier (1976). As demonstrated in Peltier (1995) these transition modes generally play a minor role in the time-domain behaviour of the h and k Love numbers but they make an important contribution to the ℓ Love number.

history of surface load variations is determined by solving the Euler equation:

$$\frac{d}{dt}(J_{ij}\,\omega_j) + \varepsilon_{ijk}\,\omega_j\,J_{k\ell}\,\omega_\ell = o \tag{9}$$

in which J_{ij} is the moment of inertia tensor of the planet, ω_j are the components of its angular velocity vector and ε_{ijk} is the Levi-Cevita alternating tensor. Since the GIA induced variations of planetary shape are small, we may employ standard perturbation theory to solve (9) by writing:

$$\begin{aligned}
\omega_i &= \Omega\,(\delta_{ij} + m_i) \\
I_{ij} &= I_{ij}\ ;\ i \neq j \\
J_{11} &= A + I_{11} \\
J_{22} &= A + I_{22} \\
J_{33} &= C + I_{33}
\end{aligned} \tag{10}$$

in which (A,A,C) are the principle moments of inertia of the (assumed) biaxial basic-state, Ω is the

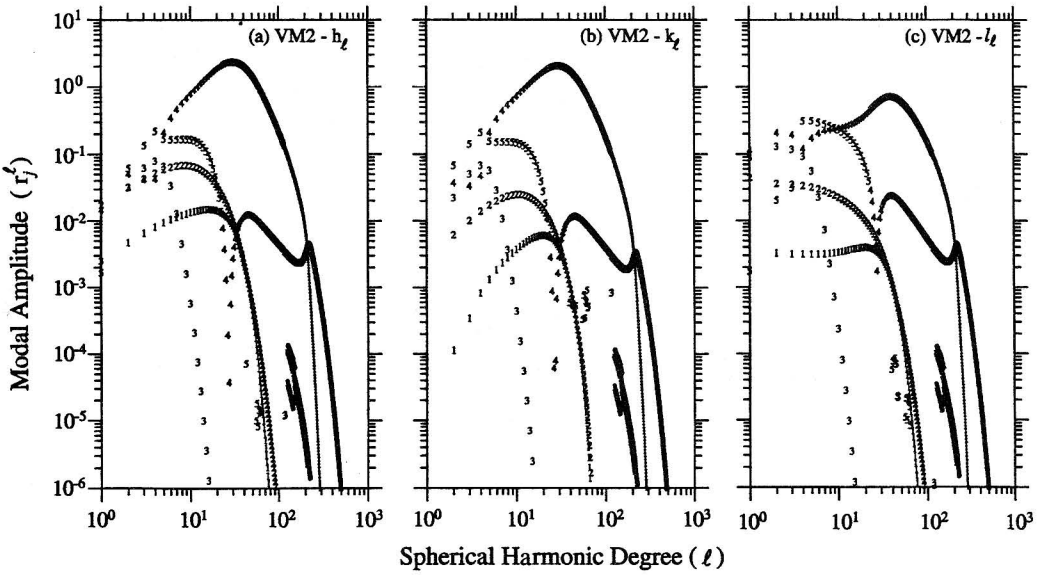

Fig. 3. Amplitude spectra of the h, k and ℓ Love numbers for viscosity model VM2 in Figure 15. The amplitudes of the individual modes have been determined using the theory of residues method described in Wu (1978) for application to simple models and extended for application to the complete compressible Maxwell model in Peltier (1985).

unperturbed angular velocity and I_{ij} and m_i are assumed small fluctuations away from these basic state values. To first order in the fluctuations (see [45]) substitution of (11) into (9) delivers the usual decoupled system of equations for the polar motion and rotation, respectively, as:

$$\frac{i}{\sigma_r}\,\underline{\dot{m}} + \underline{m} = \underline{\Psi} \tag{11a}$$

$$\dot{m}_3 = \Psi_3 \tag{11b}$$

in which the so-called excitation functions are $\underline{\Psi}$ and ψ_3, $\sigma_r = \Omega$ (C-A)/A is the Chandler wobble frequency of the rigid Earth, $\underline{m} = m_1 + i\, m_2$, $\underline{\Psi} = \psi_1 + i\, \psi_2$, $i = \sqrt{-1}$ and the ψ_i are respectively:

$$\psi_1 = \frac{I_{13}}{(C-A)} + \frac{\dot{I}_{23}}{\Omega(C-A)} \tag{12a}$$

$$\psi_2 = \frac{I_{23}}{(C-A)} - \frac{\dot{I}_{23}}{\Omega(C-A)} \tag{12b}$$

$$\psi_3 = -\frac{I_{33}}{C} \tag{12c}$$

Given a solution to (11) we are in a position to extend (2) to include the full influence of rotational feedback due to the varying rotation by modifying it into the form:

$$S(\theta,\lambda,t) = C(\theta,\lambda,t)\left[\int_{-\infty}^{\infty} dt' \iint_{\Omega} d\Omega' \left\{ L(\theta',\phi',t')\, G_{\phi}^{L}(\gamma, t-t') + \psi^{R}(\theta',\lambda',t')\, G_{\phi}^{T}(\gamma, t-t') \right\} + \frac{\Delta\Phi(t)}{g}\right], \tag{13}$$

in which two distinct Green functions and two distinct "loads" now appear. The first Green function G_{ϕ}^{L} is as in (2), namely:

$$G_{\phi}^{L} = \left[\frac{\phi(\gamma, t-t')}{g} - \Gamma(\gamma, -t')\right] \tag{14a}$$

whereas the second is, explicitly,

$$G_{\phi}^{T} = \frac{1}{g}\sum_{\ell=o}^{\infty}\left(1 + k_{\ell}^{T}(t-t') - h_{\ell}^{T}(t-t')\right) P_{\ell}(cos\,\gamma)\ , \tag{14b}$$

in which the Love numbers k_{ℓ}^{T} and h_{ℓ}^{T} are now tidal Love numbers determined as discussed in detail in [2] for the elastic problem and in Peltier [22] for the visco-elastic problem. The additional "load" that appears in (13), $\psi^{R}(\theta', \lambda', t')$, consists of the variation of the centrifugal potential caused by the changing rotation. This may be written, to first order in perturbation theory, following Dahlen [46] whose interest was in the "passive influence of the oceans on the rotation of the earth", in the form:

$$\psi^{R}(\theta,\lambda) = \psi_{oo}\, Y_{oo}(\theta,\lambda) + \sum_{m=-1}^{+1} \psi_{2m}\, Y_{2m}(\theta,\lambda) \tag{15}$$

with

$$\psi_{oo} = \frac{2}{3}\,\omega_{3}(t)\,\Omega_{o}\,a^{2} \tag{16a}$$

$$\psi_{20} = -\frac{1}{3}\,\omega_{3}(t)\,\Omega_{o}\sqrt{4/5} \tag{16b}$$

$$\psi_{2-1} = (\omega_{1} - i\,\omega_{2})\,(\Omega_{o}\,a^{2}/2)\,\sqrt{2/15} \tag{16c}$$

$$\psi_{2+1} = (\omega_{1} + i\,\omega_{2})\,(\Omega_{o}\,a^{2}/2)\,\sqrt{2/15} \tag{16d}$$

By employing the form of the Sea Level Equation (13) rather than the form (2) one may investigate the strength of the rotational feedback on rsl history. In [47] it was recently claimed that this feedback was strong and therefore that the use of the form (2) would lead to significant error. In fact, as I have shown in detail elsewhere [37], [41], [42], this influence is negligibly weak for

almost all purposes. This is important because the form (2) has been employed as basis for all of the previous work on the GIA process.

The only additional issue that warrants discussion concerning either of these forms of the Sea Level Equation concerns the methods required to incorporate the influence of time variations in the ocean function C. Whether or not the influence of changing rotation is included, the iterative procedure whereby this effect may be accurately incorporated in the analysis is precisely that described in [27], and no purpose will be served by providing a detailed review of this procedure here. For a recent review of the complete iterative algorithm the interested reader is referred to [27], [37], [40]. A brief summary will be provided below.

To end this Section, I show in Figure 4 two example solutions of the Sea Level Equation, one based upon the form (2) and the other based upon the form (13). The solutions are each represented, in plates (a) and (b) respectively, in terms of their predictions of the present day rate of relative sea level rise. Both employ the same history of deglaciation, namely the ICE-4G model of [27] in which the system is assumed to be in isostatic equilibrium at last glacial maximum (LGM, assumed to have occurred 21,000 years before present) and in which all melting is assumed to have been complete by 4,000 years ago. The glaciation history prior to LGM is constrained by SPECMAP [62]. Furthermore, both calculations employ the same model of the radial viscosity variation, namely the VM2 model shown on Figure 1. The difference between these two predictions is shown on plate (c) which therefore contains the influence of the changing rotation alone and this is observed to possess precisely the degree 2 and order 1 dominant structure expected on the basis of the first order perturbation theoretic form of the centrifugal forcing defined in equations (16). Figure 5 shows examples of complete histories of rsl from LGM to present for six different locations on the Earth's surface that might be considered illustrative of the regions where the impact of rotational feedback could be important. Inspection will show that the impact of rotation, even at the four locations where it is strongest, is extremely weak. Clearly the crude analysis of this problem reported in [47] was incorrect by approximately two orders of magnitude.

3. GIA Implications for Solid Earth Geophysics: the Continuing Saga of Mantle Viscosity

Continuing interest on the GIA process derives in large part from the fact that it provides the most direct and least ambiguous means of inferring the effective steady-state creep resistance of Earth's mantle. Since this parameter is clearly required in order to construct a thermal convection model of the sea floor spreading process, and since such models can only be successfully constructed if the viscosity lies in a rather restricted range [48], the measurement of viscosity, and thus the GIA process itself, provides a fundamental link in the logical edifice of geodynamics. Very recently it has proven possible to bring the formal apparatus of geophysical inverse theory to bear upon the problem of inferring the depth dependence of mantle viscosity from the simultaneous inversion of a wide range of different GIA related data ([49], [33], [42]), and it will prove useful to begin this Section by reviewing and extending these results.

The strategy that has been adopted in this work has been to focus the formal analysis upon

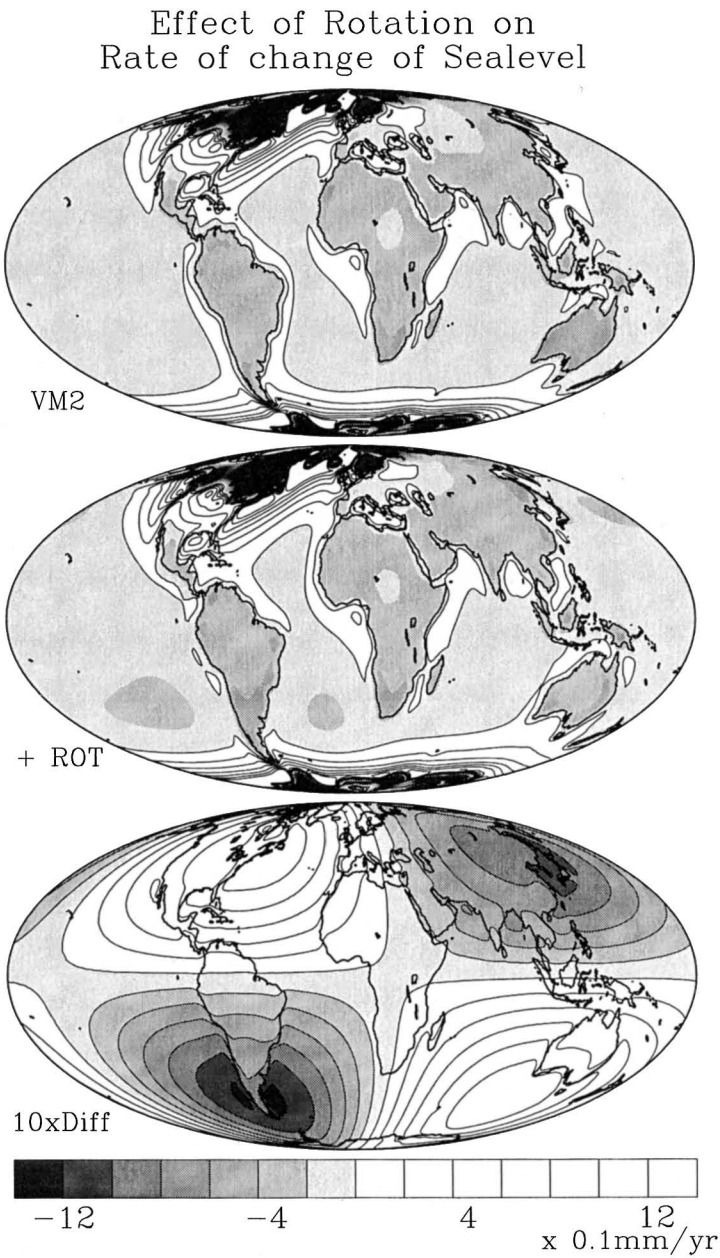

Fig. 4. Predictions of the present day rate of relative sea level rise using the VM2 viscosity model and the ICE-4G deglaciation history. Results are shown for analyses performed that both exclude (top plate) and include (central plate) the influence of rotational feedback and (bottom plate) the difference between these predictions which isolates the influence of the changing rotation alone.

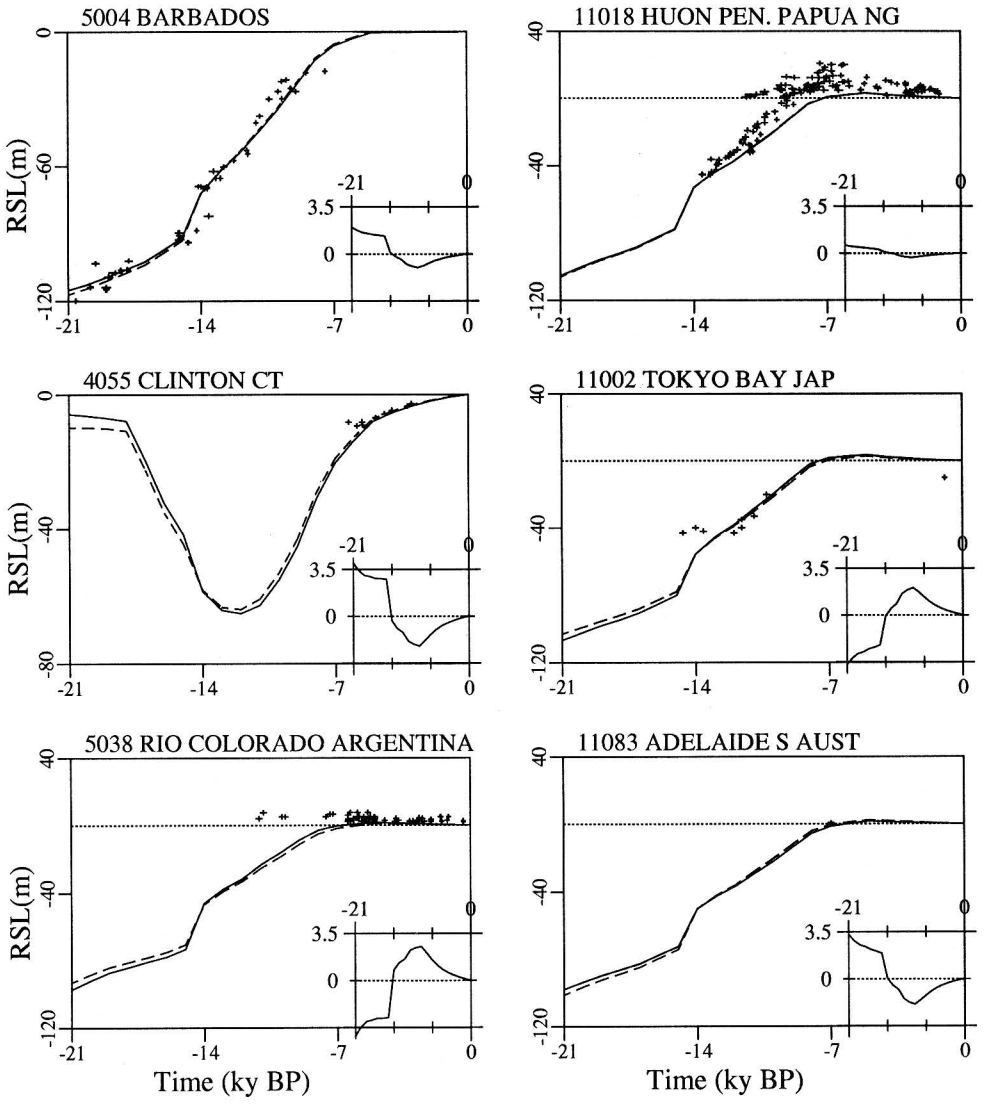

Fig. 5. Relative sea level histories at six significant locations illustrating the negligibly weak impact of rotational feedback upon the Holocene record. The Barbados and Huon Penninsula sites are the two primary locations from which coral based records are available. For the latter site only the raw data are shown, uncorrected for any influence of tectonic uplift. The final four sites are located as close as possible to the centres of the degree two and order one structure that characterizes the contribution of rotational feedback on rsl history. It is at these locations where the influence of this feedback is maximum. The solid curve in each frame represents the rsl history that includes rotational feedback whereas the dashed curve is that obtained excluding this effect. The inset in each plate represents the difference between these two histories on a scale that ranges between -3.5 m and + 3.5 m. Both sets of calculations were performed with the ICE-4G (VM2) model.

the inversion of a sub-set of the observational data that is expected to provide the best possible resolution from the base of the lithosphere to the core-mantle boundary, while reserving most of the available data for the purpose of verifying the quality of the model so determined. The first data type employed in this mix consists of site-specific relaxation times from individual locations in Canada and Scandinavia that were once covered by the Laurentide and Fennoscandia ice-sheets respectively. Examples of this type of data are provided on Figure 6 which shows radio-carbon dated rsl histories at three locations in Canada, respectively southeast Hudson Bay, Richmond Gulf (also on the east coast of Hudson Bay) and Bathurst Inlet in the Canadian high Arctic. Two representations of the southeast Hudson Bay data, which all consist of shell dates, are shown to illustrate the large impact on the rsl history that may arise due to the fact that different species may live at different depths below msl. Also shown on this Figure are the parameters A and T derived by employing a Monte Carlo procedure to determine the best fit of the exponential model $rsl(t) = A \bullet [e^{t/T}-1]$, in which t is the "age" of the specimen and t=o corresponds to the present day, to the individual time series. Because such rsl histories are recorded in the geological record only subsequent to the disappearance of land ice, when the surface is undergoing a free viscous return to equilibrium, it is clear that the relaxation time data will be minimally influenced by the actual variations of ice-sheet thickness that were responsible for inducing the depression of the surface whose recovery is recorded in the rsl history. Two additional data types will also be employed in the formal inversions. The first consists of the relaxation spectrum for Fennoscandian rebound of [55] that is shown on Figure 7 which assigns a single relaxation time to each spherical harmonic degree (or bins of spherical harmonic degree) in the range $14 \leq \ell \leq 75$ with a considerable gap in the spectrum for $\ell \simeq 40$. The final data to be employed in the formal inversions consist of the two anomalies in the rotational response mentioned in the Introduction, namely the observed "non-tidal" acceleration in the rate of axial rotation and the observed rate of "true-polar-wander" relative to the surface geography. Detailed recent discussions of these rotational constraints have appeared in [43], [44] and [37] and no useful purpose will be served by further discussing the data themselves. Figure 8, however, illustrates the fit of the theory embodied in (2) and (9) to these observations for a sequence of simple two layer viscosity models of the depth variation of this parameter through the planetary mantle. With the lithospheric thickness fixed to 120.6 km and the upper mantle and transition zone viscosity fixed to 10^{21} Pa s, theoretical predictions of the rotational data are shown as a function of the lower mantle viscosity ν_{LM}. On each plate of this Figure the horizontal hatched region indicates the range of the observation. Inspection of these results will demonstrate that when the ICE-4G model is employed to represent the history of deglaciation (several cycles of 100 kyr glaciation and deglaciation have also been included for the purpose of this calculation) then both rotational data are fit by exactly the same two layer model of the viscosity stratification, namely the model labelled VM1 on the previously described Figure 1. Given that the two rotational data sample completely orthogonal elements of the tensor of inertia perturbations, I am on this basis inclined to argue very strongly that both rotational anomalies must in fact be due to the GIA process and that the actually profile of mantle viscosity must be "linearly close" in some "logarithm of viscosity sense" (see below) to the profile VM1. Inspection of Figure 7, however, will show that model VM1 does not fit the McConnell relaxation spectrum for Fennoscandian rebound. In order to determine the profile (or family of profiles) that might best reconcile the totality of the data we clearly require a formal procedure that may be employed to properly trade-off the relative influence

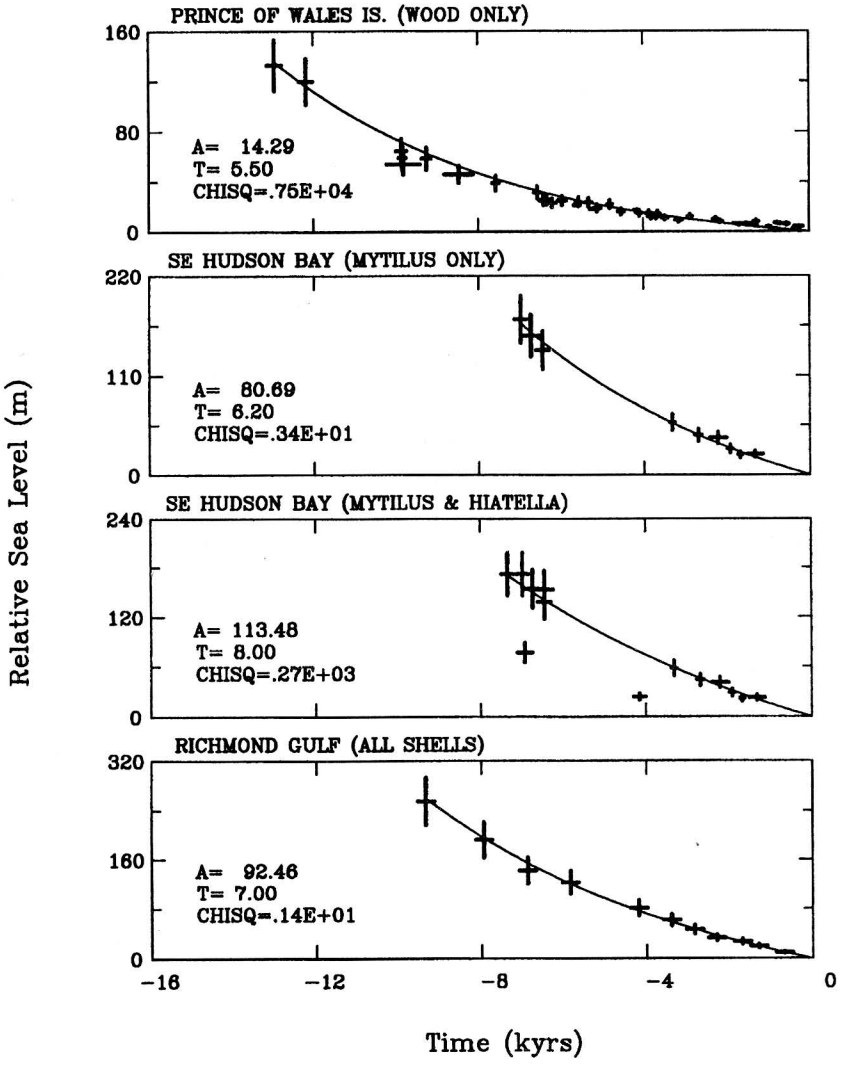

Fig. 6. Examples of ^{14}C dated relative sea level records from three different locations in Canada, together with the fits to these data obtained by employing a Monte Carlo technique to determine best estimates of the amplitude A and relaxation time T in a fit to the data of the exponential model rsl(t) = A [exp (t/T)-1] in which t is sample age in sidereal years. In plotting the ^{14}C data on Figures such as this, and for the purpose of determining the A and T variables that may be employed to characterize the postglacial rebound process that is ongoing at sites that were once ice-covered, sample age in ^{14}C years is mapped to sidereal age using the calibration of Bard et al. (1990). The curves for the individual named sites are discussed in the text.

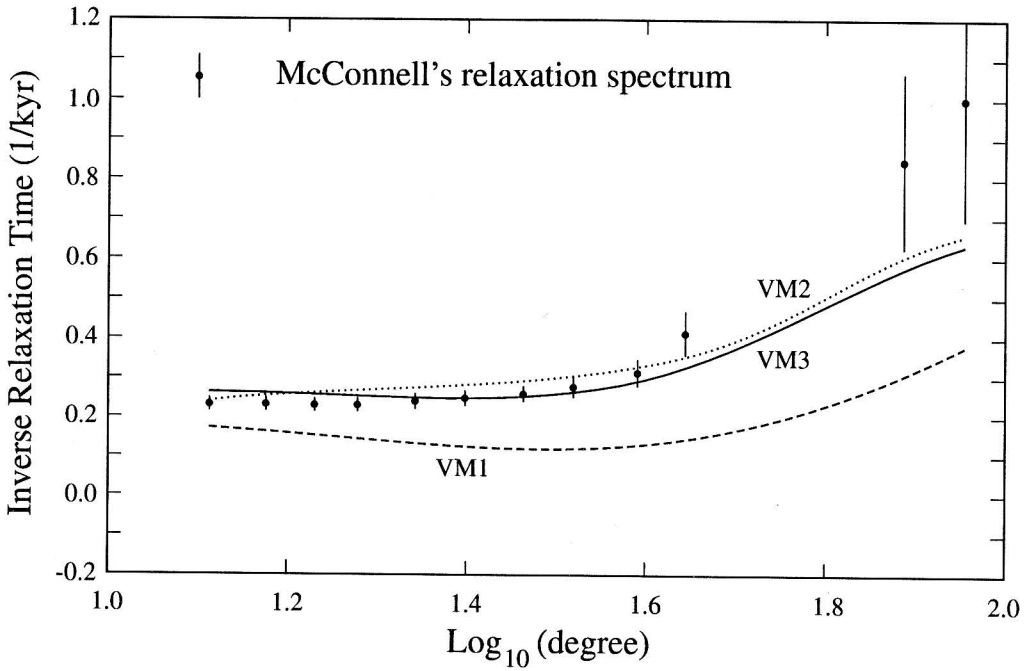

Fig. 7. The relaxation spectrum for Fennoscandian rebound of McConnell (1968) along with predictions of this spectrum for models VM1, VM2 and VM3. Note that model VM1 predicts relaxation times that are in excess of those inferred by McConnell at every spherical harmonic degree. Models VM2 and VM3, on the other hand, fit the observed spectrum nicely. Note that the error bars assigned to the relaxation time observations of McConnell may be somewhat overly optimistic. However, it is clear that at lowest wavenumber must one have a relaxation time that agrees with the site-specific relaxation time at the Angermanland River location (shown as the star), which is very close to 4000 years, and on this basis, since the long wavelength asymptote of the McConnell spectrum does indeed fit this observation, I have supposed it mandatory that the inferred viscosity models should fit this spectrum to within the 10% error bounds shown. Again, this may be somewhat excessively confining.

of the different types of information.

Basic to such an analysis, in the event that we are indeed in a position to assert that the profile VM1 is linearly close to the "correct" solution(s), is the Fréchet derivative which describes the sensitivity of the forward predictions of the theoretical model (in this case (2) plus (9)) to variations in the viscosity structure of the mantle. If R is some measure of the response of the model then the Fréchet kernel $FK^R(r)$ is the functional derivative that appears in the equation:

$$\delta R = \int_b^a FK^R(r)\, \delta \log \nu(r)\, dr \,, \tag{17}$$

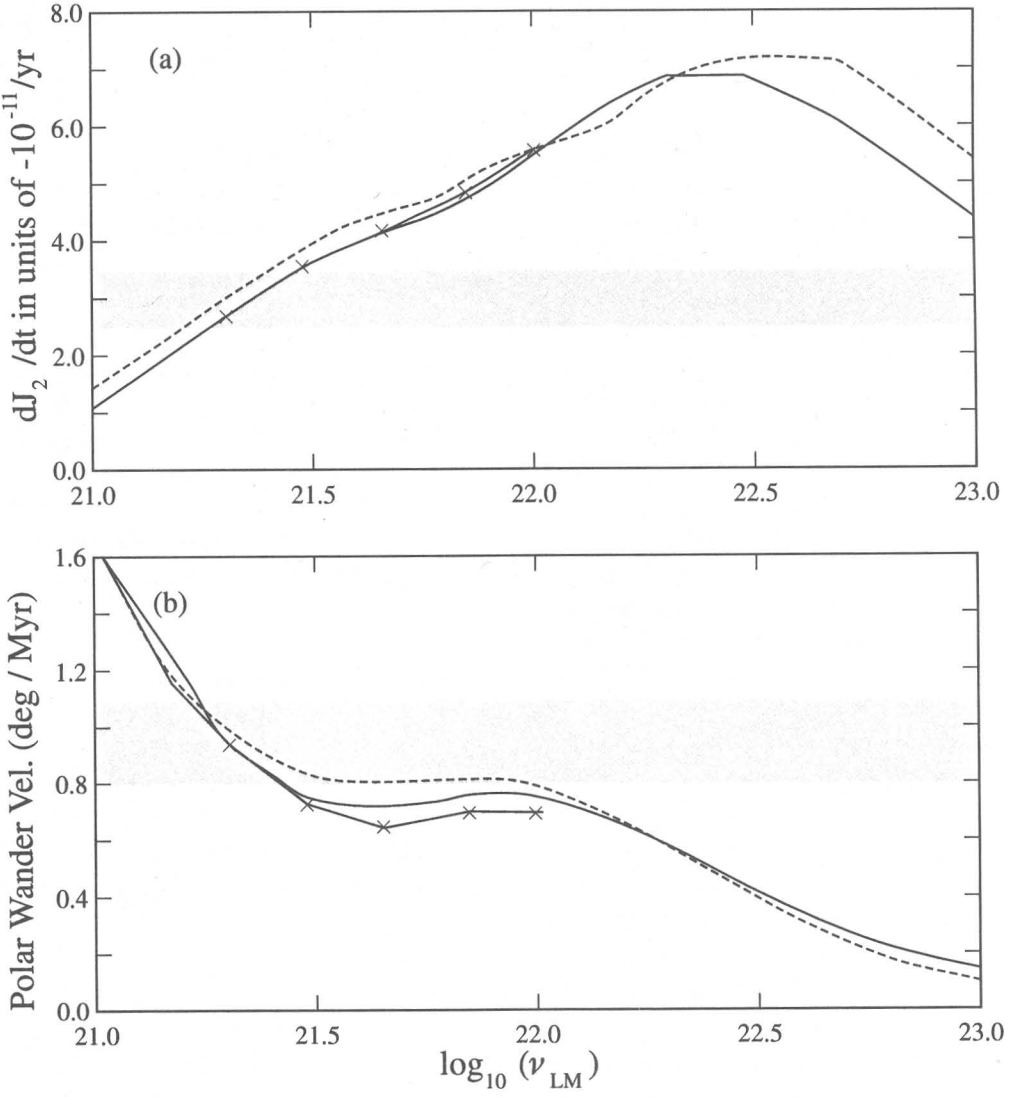

Fig. 8. (a) $\dot{J}_2$ as a function of lower mantle viscosity ν_{LM} when the upper mantle and transition zone viscosity is fixed to the value $\nu_{UM} = 1.0 \times 10^{21}$ Pa s and the lithospheric thickness is L = 120.6 km. Results are shown for both of the models of glaciation history for which inertia perturbations are shown in Figure 33. (b) Polar wander speed as a function of lower mantle viscosity ν_{LM} with other parameters as in (a).

in which the viscosity model $\nu(r)$ is "parameterized" in terms of its logarithm (to the base 10), this parameterization being strongly suggested by the fact [4] that the use of it to define FK^R as in (17) strongly linearizes the inverse problem. What this means in practise is that the FK^R defined in this

way and evaluated "at" the starting model (VM1, say) may be employed to predict the δR induced by a perturbation in viscosity for rather large variations in viscosity (typically by an order to magnitude or more).

The reason for our choice of the specific types of data to be employed for the purpose of formal inversion will be clear on the basis of Figure 9 which shows examples of the FK^R for the three types of data described at the beginning of this Section. To compute Fréchet "kernels" associated with the McConnell relaxation time data for Fennoscandian rebound shown on plate (a), I have employed the analytical functional form for the kernels derived in [10] based upon a viscoelastic extension of Rayleigh's variational principle of elasticity. For the site specific relaxation time data from both Canada and Fennoscandia, however, example Fréchet kernels for which are shown in plate (b), and for the rotational data with Fréchet kernels shown on plate (c), the Fréchet derivatives must be computed numerically by using equation (17). One simply adds delta-function-like perturbations to the viscosity structure of the "starting-model", which we will take to be VM1 based upon the previous discussion, and then solves the forward problem to determine the impact of the viscosity perturbation on the response δR. Inspection of the kernels shown on Figure 9 will show that the McConnell data provide sensitivity to upper mantle and transition zone viscosity, the site specific relaxation times from central Fennoscandia and Laurentia provide sensitivity to the transition zone and the upper part of the lower mantle respectively, whereas the rotational data display sensitivity to the viscosity structure from the upper mantle to the core-mantle boundary. Taken together the three data types would therefore appear to offer the best possible opportunity to resolve the spherically symmetric viscosity structure in an optimal fashion. Caveats to this must, however, be kept clearly in mind, namely (1) that the shallow viscosity structure will be characteristic of sub-cratonic regions above which the two main centres of glaciation were located and (2) that the deep structure that is primarily constrained by the rotational data will better represent a volume average than the structure characteristic of a particular geographical region.

Given the functional derivatives $FK^R(r)$ for each of these data types, there are a variety of methods that may be employed to map the misfits of the predictions of the forward model to the observational data into a modification to the starting viscosity model VM1. In all of the recent work that my students and I have done on this problem I have elected to employ the Bayesian methodology of [50], [51], [52] and [53]. Application of this methodology delivers what is often referred to as a "Maximum Likelihood" solution which is, effectively, a "smooth" if not a "smoothest" model that is compatible with the observations. Since this methodology has been described in great detail in these references no useful purpose will be served here by repetition. Rather, Figure 10 simply presents a series of the results that have been obtained by applying variations of the basic analysis procedure. In plate (a) is shown the starting model VM1 along with two variants of the model VM2 that is obtained by applying the Bayesian formalism to the previously described data. The two versions of VM2 differ only in the way in which the site-specific relaxation time observations have been treated. In obtaining the model shown as the heavy solid line, the observed relaxation times were obtained by Monte Carlo fit to the envelope sampled form of the radio-carbon data compiled in [54], whereas for the model represented by the thin solid

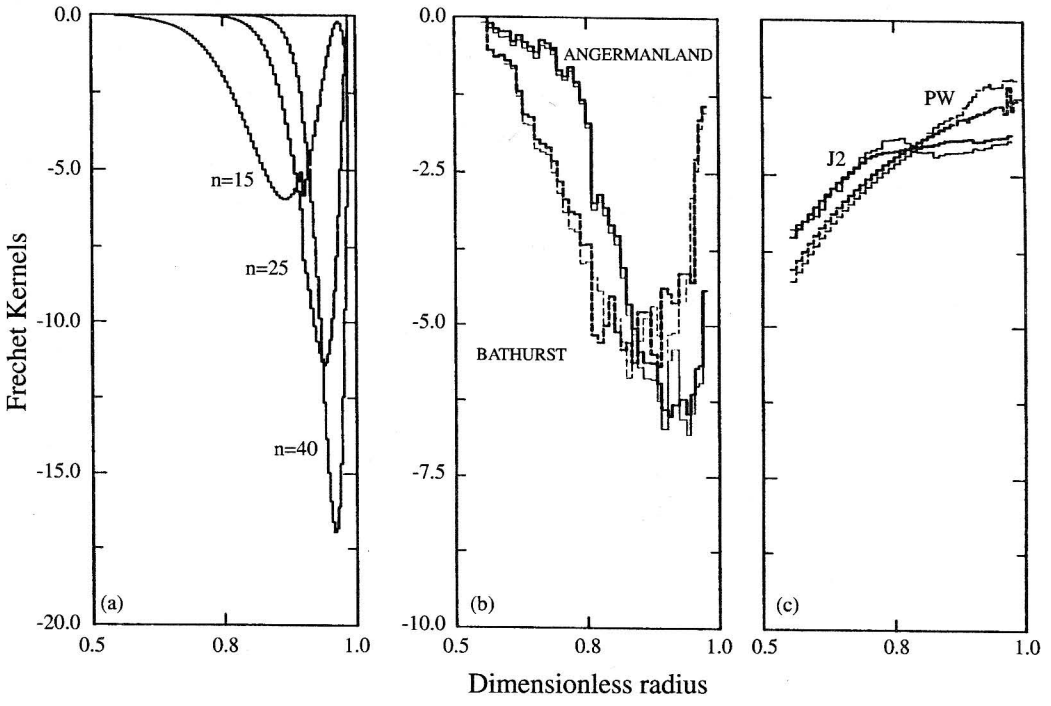

Fig. 9. Fréchet derivatives for a representative set of the data related to the GIA process. Plate (a) shows a sequence of kernels for the inverse relaxation times of a number of spherical harmonic degrees of the McConnell relaxation spectrum based upon the analytic formula in Peltier (1976). Plate (b) shows Fréchet derivatives for the site specific relaxation times at sites near the center of Laurentide rebound (Bathurst Inlet - this is actually a high Arctic site) and at the center for Fennoscandian rebound (the Angermanland River site). Plate (c) shows kernels for the non-tidal acceleration of rotation ($\dot{J}_2$) and polar wander speed (PW) that were determined numerically using the procedure embodied in equations (21) and (22) of the text. Inspection of this suite of kernels, all of which were computed on model VM1 that is employed as starting model in the Bayesian inversions, demonstrates that the observables whose sensitivity to viscosity variations they represent, offer the potential of significant resolution from the Earth's surface to the cmb.

line the site-specific relaxation times were based on Monte Carlo fits to the raw data. Inspection of the Figure shows that these two variants on the analysis procedure do not lead to any significant difference in the inferred viscosity profile. In plate (b) is shown a further version of the VM2 model which differs from the previous two in that, for the purpose of the forward prediction of the site specific relaxation times, the full influence of the time dependence of the ocean function was included, an effect that was suppressed in the previous analyses. Again, inspection of this further version of VM2 shows that it differs in no important way from those previously obtained, a slight increase in the average viscosity of the upper part of the lower mantle being the sole effect.

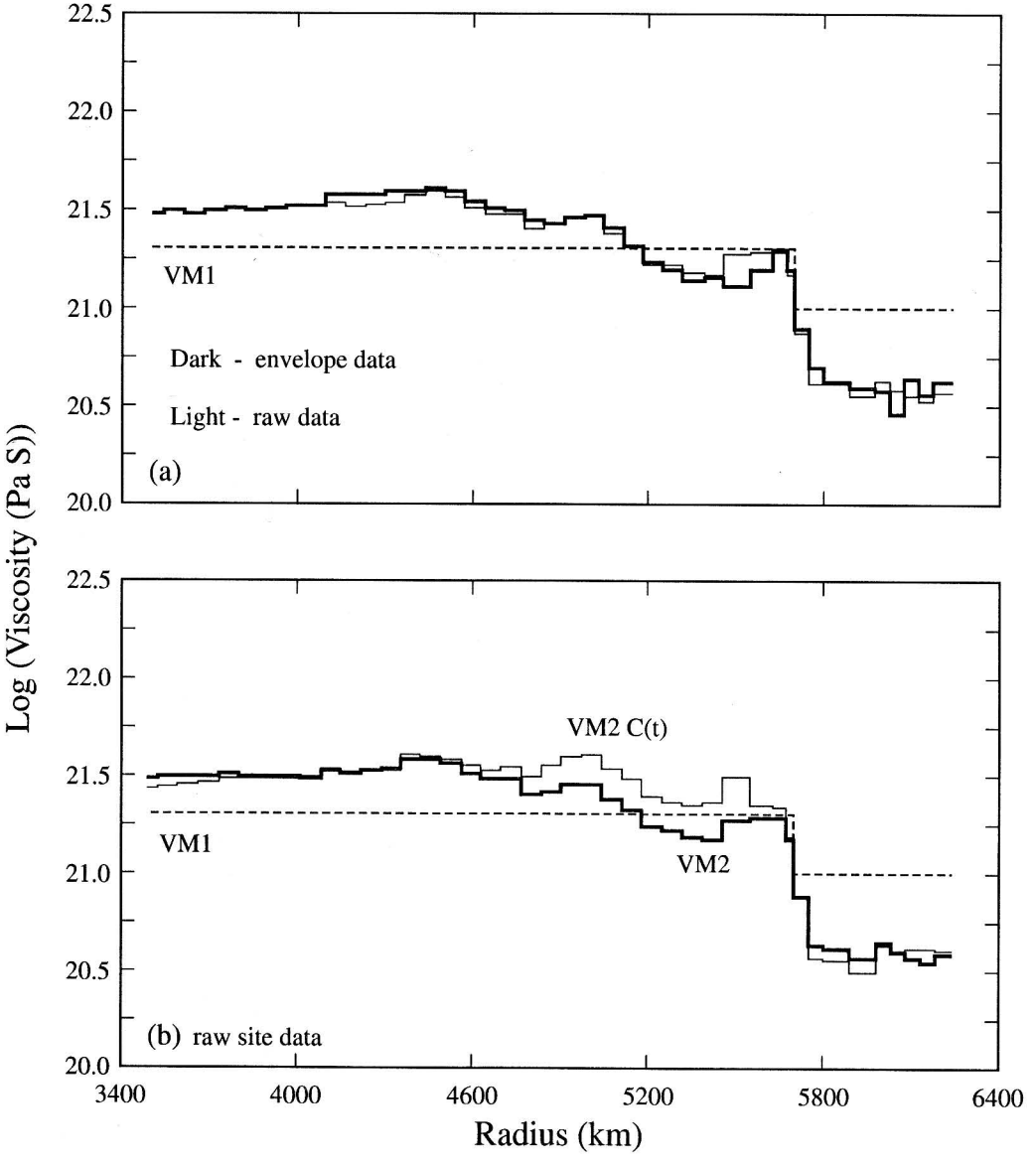

Fig. 10. Viscosity profiles determined by simultaneous formal Bayesian inversion of the Fennoscandian relaxation spectrum of McConnell (1968), the site specific relaxation times from 23 ice covered sites in Canada and Fennoscandia and the non-tidal acceleration of the rate of axial rotation. In (a) the dashed line is the VM1 viscosity profile employed as starting model in the inversion process while two versions of the final model are shown as the dark and light solid lines respectively, these being distinct versions of VM2. The former of these two inferred models has been obtained using site specific relaxation times obtained from fits to the envelope sampled data compiled by Tushingham and Peltier [54] whereas the latter was obtained on the basis of - Cont.

Now it is important to realize, as mentioned previously, that the maximum likelihood models delivered by application of the Bayesian formalism are in a real sense among the smoothest models that are compatible with the data although no explicit penalty against "roughness" was applied in performing the inversions. Returning to consideration of Figure 7, the manner in which the profile VM1 was adjusted by the formalism will be clear. Because VM1 did not fit the McConnell relaxation spectrum for Fennoscandia, the viscosity in the upper mantle and transition zone had to be slightly reduced, by approximately a factor of 2 to an average near 0.5 x 10^{21} Pa s. In the upper part of the lower mantle, however, the viscosity was held close to the value of 2 x 10^{21} Pa s which characterized this region in VM1 because the forward predictions of the site specific relaxation times for Canada which are sensitive to precisely this region were well fit by VM1. In order to compensate for the reduction in the viscosity of the upper mantle and transition zone, therefore, the rotational datum ($\dot{J}_2$) employed in these inversions requires that the viscosity in the deepest part of the lower mantle be slightly increased. The result is the VM2 sequence of models. That these models cannot be considered to be, in any sense, unique, may best be illustrated by providing a specific example. I will focus here on one that is best motivated by consideration of Figure 11 which shows an overlay of a further version of the viscosity profile obtained by inverting the GIA data, specifically the model denoted VM3 in Figure 1, with a viscosity profile recently inferred in [56] and [57] on the basis of the inversion of the non-hydrostatic geoid anomalies related to the mantle convection process. As discussed in [49], VM3 is obtained by modifying the $\dot{J}_2$ datum to account for the influence of a contribution to the ongoing rise of global sea level due to the melting of polar ice sheets. Inspection of this Figure will show that the VM3 model and the geoid derived model are essentially identical except in a thin layer 70 km thick that overlies the 660 km seismic discontinuity and in which the viscosity is reduced by a factor of approximately 30. The issue is whether the GIA data can accommodate a dramatic feature of this type.

That this feature is in fact easily accommodated by the GIA data will be clear on the basis of the information presented in Figure 12. In plate (a), I illustrate the impact upon the forward model prediction of the McConnell relaxation spectrum for "perturbed" versions of the VM2 model to which a 70 km thick low viscosity channel has been added in which the viscosity is assumed to be either 10^{20} Pa s or 10^{19} Pa s. In either case it will be clear that the predicted spectrum no longer fits the McConnell observations and therefore it might appear that the existence of such a feature is ruled out by Fennoscandian rebound data. That this is not in fact the case is made clear in plate (b) of Figure 12 in which it is demonstrated that a slight elevation of the viscosity of the mantle in the transition zone is sufficient to eliminate the misfit induced by the presence of the soft

Fig. 10 continued site specific relaxation times deduced from the raw data themselves. In (b), where the dashed line also indicates VM1, the two versions shown of the final model are VM2 (that based upon use of the raw data to determine the site-specific relaxation times) and a further version in which the starting model predictions were made with the version of the model that included the full influence of time dependence of the ocean function. Incorporation of the latter effect in the forward model slightly decreases the forward predictions for the site specific relaxation times and therefore slightly increases the inferred viscosity in the upper part of the lower mantle, essentially back to the value of 2 x 10^{21} Pa s that is characteristic of the starting model VM1 in this region.

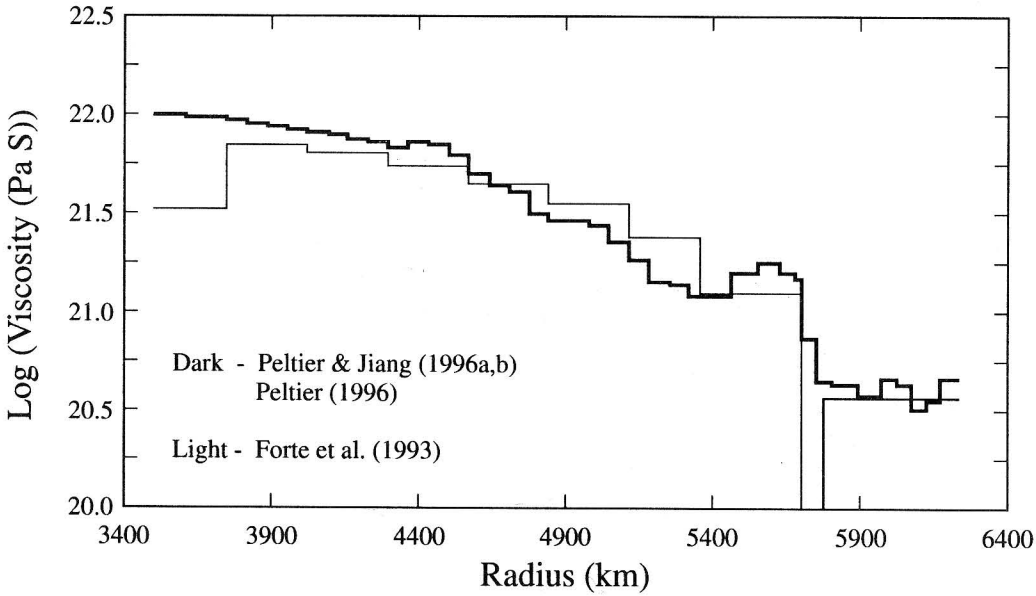

Fig. 11. Overlay of the mantle viscosity profile VM3 deduced on the basis of inversions of the GIA data and the profile inferred by Fort et al. (1993) and Pari and Peltier (1995) based upon the inversion of non-hydrostatic geoid data.

layer alone. Since the transition zone is rich in garnet and since this is expected to significantly increase the bulk creep resistance one might argue that models of this kind, which simultaneously reconcile both non-hydrostatic geoid and GIA data, are especially compelling. It could well be, however (see [58]), that the preference of the geoid data for models with a low viscosity channel on or above the 660 km discontinuity is a consequence of errors in the seismic tomography based inferences of the mantle density heterogeneity. It is an unfortunate fact [58] that the inference of mantle viscosity on the basis of the non-hydrostatic geoid data is rendered extremely non-robust because of the profound sensitivity of the viscosity inference to seismically undetectable modifications to the tomography models.

In completing this brief discussion of the implications of the GIA data for understanding the physics of the solid Earth, I will consider briefly the nature of the predictions of three-dimensional displacement rates which have very recently become amenable to space-geodetic observation. Given a solution to either version (2) or version (9) of the Sea Level Equation we have complete knowledge of the space-time variation of the surface load L and we may therefore compute the time dependent radial and tangential components of displacement at the surface of the solid Earth by convolution of this surface load, with its ice and water components, with appropriate Green functions. The most accurate way to evaluate these a-posteriori convolution integrals is to employ the spectral formalism of [10] that is simply based upon the so-called convolution theorem through which it is demonstrated that space-domain convolution is equivalent to wavenumber

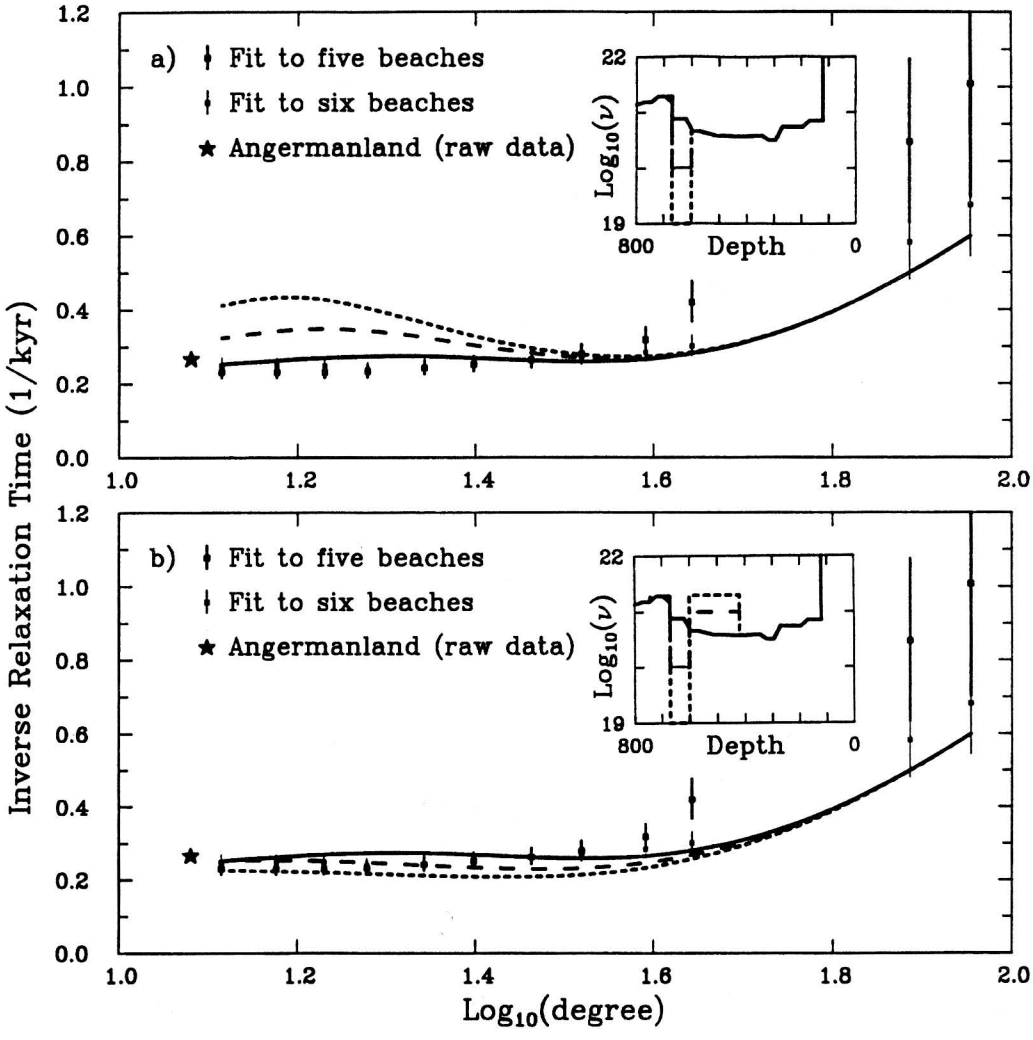

Fig. 12. (a)The inverse relaxation time spectrum for Fennoscandian rebound of McConnell (1968) compared to the prediction of a model in the VM2 class and compared to the predictions for two additional models that differ from VM2 by the presence of a 70 km thick layer immediately overlaying the 660 km discontinuity in which the viscosity is reduced either by one or two orders of magnitude from the value near 0.45 x 10^{21} Pa s that otherwise obtains in this region of VM2.

domain multiplication. This yields expressions for the radial displacement scalar U and the tangential displacement vector $\underline{V}$ as:

$$U(\theta,\lambda,t) = \sum_{\ell=o}^{\infty} \sum_{m=-\ell}^{+\ell} \left[\frac{4\pi a^3}{(2\ell+1)\, m_e} \left(L_{\ell m} h_\ell^E + \sum_{k=1}^{k(\ell)} q_k^\ell q_k^\ell \beta_{\ell m}^k \right) \right] Y_{\ell,m} \tag{18a}$$

$$\underline{V}(\theta,\lambda,t) = \sum_{\ell=o}^{\infty} \sum_{m=-\ell}^{+\ell} \left[\frac{4\pi a^3}{(2\ell+1)\, m_e} \left(L_{\ell m} \ell_\ell^E + \sum_{k=1}^{k(\ell)} t_k^\ell \beta_{\ell m}^k \right) \right] \underline{\nabla} Y_{\ell m} \tag{18b}$$

in which m_e and a are respectively the Earth's radius and mass, $L_{\ell m}(t)$ are the time dependent spherical harmonic components of the surface mass load and the $\beta_{\ell m}^k$ are the functions introduced in [59] to allow one to accurately account for an arbitrary history of surface mass loading. They are explicitly

$$\beta_{\ell m}^k(t) = \int_{-\infty}^{t} L_{\ell m}(t')\, e^{-s_k^\ell (t-t')}\, dt' \ . \tag{19}$$

In (18) the $Y_{\ell m}$ are the usual spherical harmonic basis functions and the form $\underline{\nabla}\, Y_{\ell m}$ that appears in the expression for the tangential displacement (18) may be evaluated using the explicit expression provided in [60] as it was in [9].

In producing Figure 13, I have evaluated equations (18) over both Northwestern Europe and North America using the ICE-4G deglaciation model of [27] and for both the VM1 and VM2 viscosity models. In performing the analyses over Fennoscandia the slight variant on the ICE-4G model derived in [33] was used in conjunction with the VM2 viscosity model. Inspection of the results shown on Figure 13 will demonstrate that, although the impact upon the horizontal motion prediction in Northwestern Europe of the VM1 -> VM2 viscosity profile "switch" is small, no doubt due to the rescaling of the load required to maintain the fit to the vertical motion observations over the ice covered region, the same is not the case over the North American continent. In this region the softer upper mantle and transition zone in VM2 leads to a marked increase of the rate of outward motion predicted to be occurring at present. As recently suggested in [32], this signal is sufficiently large that it should be detectable in a suitably long term GPS campaign of the type that has recently proven to be so successful in Fennoscandia. This is potentially an extremely important result as it has been clearly demonstrated that the VM2 model is strongly preferred over VM1 on the basis of both radio-carbon based rsl data from sites along the eastern coast of the continental United States ([33], [39]) and also on the basis of space-geodetic VLBI observations [61]. Tentative analyses reported in [61], however, suggest that the tangential motion observations exhibit preference for the much weaker tangential motion signal that is characteristic of VM1. If this preference should be confirmed by the further analyses that are ongoing, further modification to the basic VM2 viscosity structure will clearly be required, perhaps involving an adjustment of lithospheric thickness.

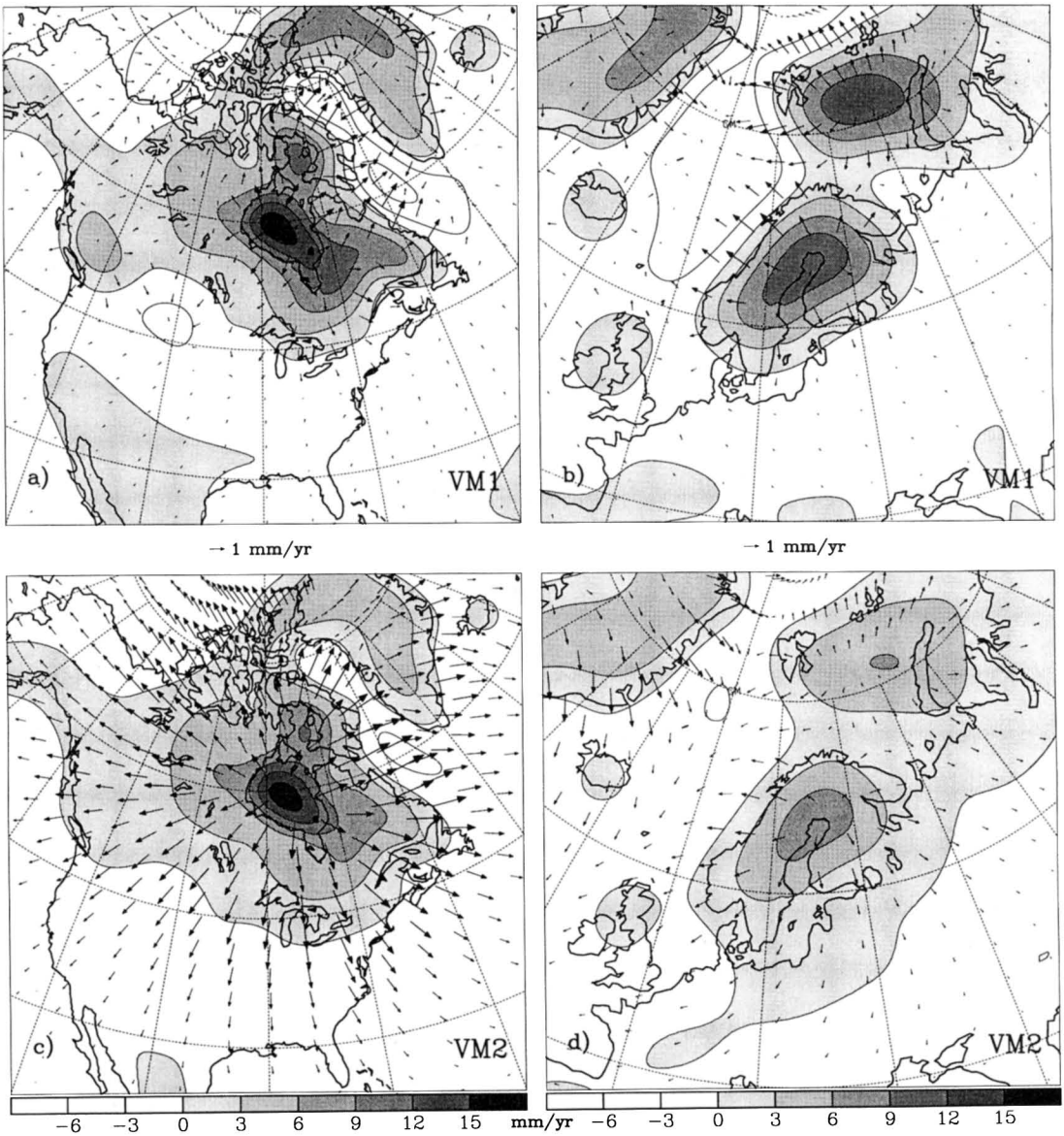

Fig. 13. Superimposed fields of the present day rate of radial displacement $\dot{U}$ and horizontal displacement $\underline{\dot{V}}$ over both Laurentia and Fennoscandia for the ICE-4G (VM1) and ICE-4G (VM2) models.

4. GIA Implications for Climate System Dynamics

Although the above discussed applications of GIA data to the understanding of important

issues in solid Earth geophysics continue to dominate the scientific agenda in this area, in the recent past it has become increasingly clear that these data also contain important paleoclimatological information. Probably of greatest importance from this perspective are the inferences of LGM ice sheet thickness that may be obtained using postglacial relative sea level histories from sites that were ice covered at LGM. Examples of such "rebound" data were shown previously in Figure 6. In discussing the inverse problem for mantle viscosity, I argued that the relaxation times derived on the basis of Monte Carlo fits of an exponential relaxation model to such data provide important constraints on the radial variation of mantle viscosity. Likewise the amplitude information deduced in the same process depend essentially upon ice-sheet thickness and its variations with time and so may be employed to constrain the amount of ice that must have existed over the main centres of glaciation. The accuracy with which the amplitude data may be employed for this purpose depends upon the validity of a number of assumptions. Primary among these is that one may safely assume that the system consisting of ice + ocean + solid earth was in a state of isostatic equilibrium at LGM. That this is a reasonably accurate assumption, if the VM2 viscosity model is essentially correct, will be clear by inspection of Figure 14 which shows comparisons of predicted rsl histories for four sites in Canada and four in Northwestern Europe. Analyses have been performed using equation (2) which either assume that glacial isostatic equilibrium existed at LGM (with or without time dependent ocean function) or that the prehistory of glaciation and deglaciation is constrained by the SPECMAP $\delta^{18}0$ record of [62]. Comparison of the three predictions at each site demonstrates that the degree of disequilibrium that is expected to have existed at LGM is extremely slight if the VM2 viscosity model is acceptably close to reality.

Also important, however, if postglacial rebound (pgr) data are to be employed to infer ice-sheet thickness, is that strong constraints are available on the timing of deglaciation in each glaciated region and on the total mass of ice that melted from all regions combined. Although imperfect, the timing of ice sheet retreat from the main centres of Northern Hemisphere glaciation (Canada and Fennoscandia) is well constrained by radio-carbon dating of the terminal moraines that formed as the ice-sheets withdrew from their positions of full glacial extent. Furthermore, a very strong constraint exists on the total mass of ice that melted across the last glacial-interglacial transition, primarily in the form of the LGM to present coral based sea level history from the Island of Barbados in the Caribbean sea. This record, based upon the work of [63] and [64], is shown in Figure 15 where it is compared with the prediction of the ICE-4G (VM2) model of the GIA process. These data clearly establish that LGM sea level was depressed at this location by an amount near 120 metres and that the ICE-4G (VM2) model fits the observation. The significance of the existence of this global constraint on ice amount will be clear on the basis of the fact that no suitable rsl data exist with which the thickness of LGM ice on Antarctica might be inferred. All we have available from the Antarctic continent are the terminal moraines themselves, indicating that considerable excess LGM ice also existed in this region. Since this is the only glaciated region from which no suitable rsl data are available, knowing the amounts that were removed from the other locations and the total amount from Barbados one may therefore determine the amount that must have been removed from Antarctica. This is the method that was used to infer the magnitude of the deglaciation event that occurred in (primarily West) Antarctica in constructing the ICE-4G model.

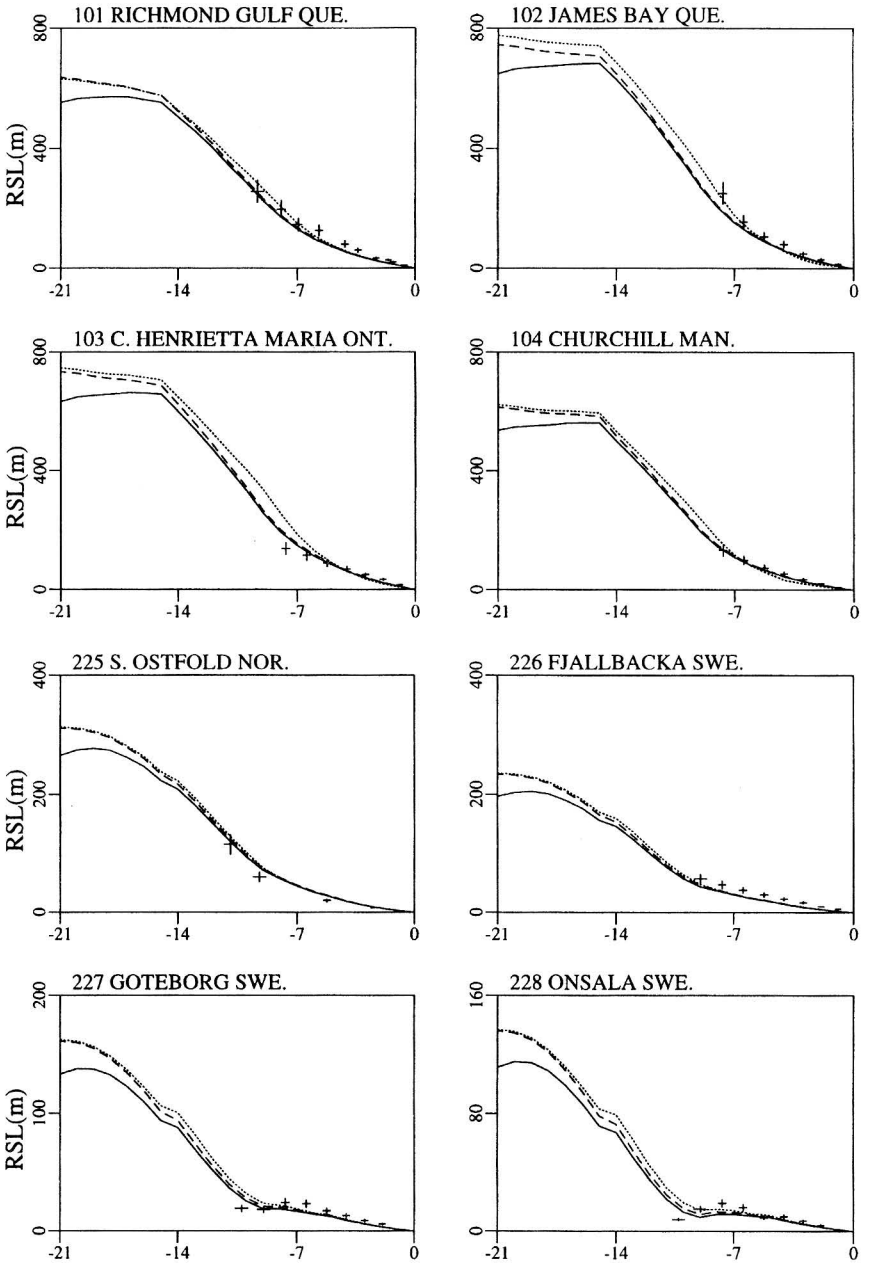

Fig. 14. Comparisons between ICE-4G (VM2) predictions of rsl history at four sites in Canada and four sites in Fennoscandia. The dashed and solid lines are predictions based upon the assumption of time independent ocean function, the former assuming initial isostatic equilibrium and the latter employing SPECMAP control glacial prehistory. The dotted line incorporates the influence of time dependent ocean function on the calculation that assumes initial isostatic equilibrium.

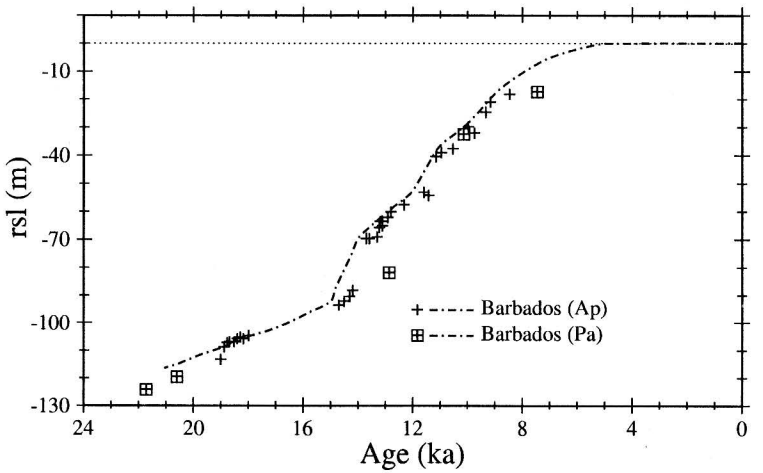

Fig. 15. The U/Th dated coral based record of postglacial relative sea level change of [63] and [64] which extends from Last Glacial Maximum (LGM) and which shows sea level to have been depressed by approximately 120 m at LGM. The data have not been corrected for tectonic uplift and they are compared on the Figure to the prediction of the ICE-4G (VM2) model. These data were in fact employed to tune the model in order to refine the temporal control on the bulk rate at which water from all sites of deglaciation enters the oceans. Primary time control on the disintegration of the Northern Hemisphere ice-sheets is of course provided by ^{14}C dates on the terminal moraines that developed during the retreat phase.

From the perspective of climatology, however, far more important than ice thickness is the height of the surface above mean sea level and the variation of this "topography" through time. Given the variation of ice-sheet thickness $I(\theta, \lambda, t)$ it is in fact possible to accurately infer this time dependent "paleotopography" as demonstrated in [27]. The subtlety that enables this calculation to be performed relies on the fact that the Sea Level Equation (either of the forms (2) or (9)) is a construct of first order perturbation theory which delivers a solution for relative sea level history with respect to an arbitrary datum. This gravitationally self-consistent solution may be made topographically self-consistent by choosing a specific datum to which sea level is to be referred. We simply define a time independent function $T'(\theta, \lambda)$ such that

$$S(\theta, \lambda, t_p) + T'(\theta, \lambda) = T'_p(\theta, \lambda) \tag{20}$$

in which $T'_p(\theta, \lambda)$ is the present day topography (defined, say, by the ETOPO 5 model) with respect to present day sea level and t_p is the present time. The field T' is then just

$$T'(\theta, \lambda) = T'_p(\theta, \lambda) - S(\theta, \lambda, t_p) \ . \tag{21}$$

If we then compute

$$T_p(\theta,\lambda,t) = S(\theta,\lambda,t) + T'(\theta,\lambda) + I(\theta,\lambda,t) \tag{22}$$

then where T_p is positive we have land (perhaps ice-covered) and where T_p is negative we have ocean. This enables us to obtain a first approximation to the ocean function $C(\theta, \lambda, t)$. We therefore solve (2) or (9) iteratively by first assuming $C(\theta, \lambda, t) = C_p$, the present day ocean function. From this solution we compute T_p (θ, λ, t) from (22) and thus C_1 (θ, λ, t). We then solve (2) or (9) again using C_1 (θ, λ, t) to determine a new paleotopography $T_p(\theta, \lambda, t)$ from (22) and continue until convergence is achieved. An example of the time varying paleotopography computed in this way is shown on Figure 16 for several instants of time. Inspection of this Figure will show that the topographic height above sea level of the Laurentide ice sheet centred on Hudson Bay was just over 2 km at LGM. This is in accord with the fact that the LGM thickness of the Laurentide ice-sheet in ICE-4G is just over 3 km. Because the surface sinks under the weight of the load by an amount equal to (ρ_I/ρ_E) I_{max}, where ρ_I is ice density and ρ_E is Earth density, we expect the surface to be depressed by ~1 km in order that the buoyancy force induced by the surface deflection balance the weight of the load.

Ice-age paleotopography that may be accurately inferred on the basis of (22) is extremely important from a climate dynamics perspective, as mentioned briefly in the Introduction to this paper. In the use of general circulation models to reconstruct past climate states, topography is a critical boundary condition. The time dependent paleotopography associated with the ICE-4G (VM2) model is currently in use in the context of the Paleoclimate Model Intercomparison Project (PMIP). Since it differs significantly from the inferences of topography developed previously in the context of the CLIMAP project, it should not be surprising that the state of the climate system predicted by such models for the LGM "time slice" is somewhat different then previously imagined. Detailed discussions of this fact will be published elsewhere (see [34] for PMIP simulations of the mid-Holocene warm period).

In completing this very cursory review of some aspects of GIA contributions to the understanding of climate system dynamics, I will focus briefly on one other significant impact that paleotopography appears to exert. This concerns the 100 kyr cycle of ice-age recurrence itself. The model of the ice-age cycle that my students and I are continuing to develop at Toronto consists of two interlinked elements, respectively an energy balance model of the atmosphere which incorporates a geographically accurate description of the continents and oceans and a model of ice-sheet accumulation and flow. Each of these elements of the theoretical structure consists of a nonlinear diffusion equation. Specifically, the surface energy balance is described by the equation:

$$C(\underline{r})\frac{\partial T}{\partial t} = \left\{\frac{Q}{4}a(\underline{r},t)\,S'(\theta,t) + \mathrm{NAHF}(\underline{r},t)\right\} - \left\{A + B\,T(\underline{r},t) - \underline{\nabla}_h\left[D(\theta)\underline{\nabla}_h T(\underline{r},t)\right]\right\} \tag{23}$$

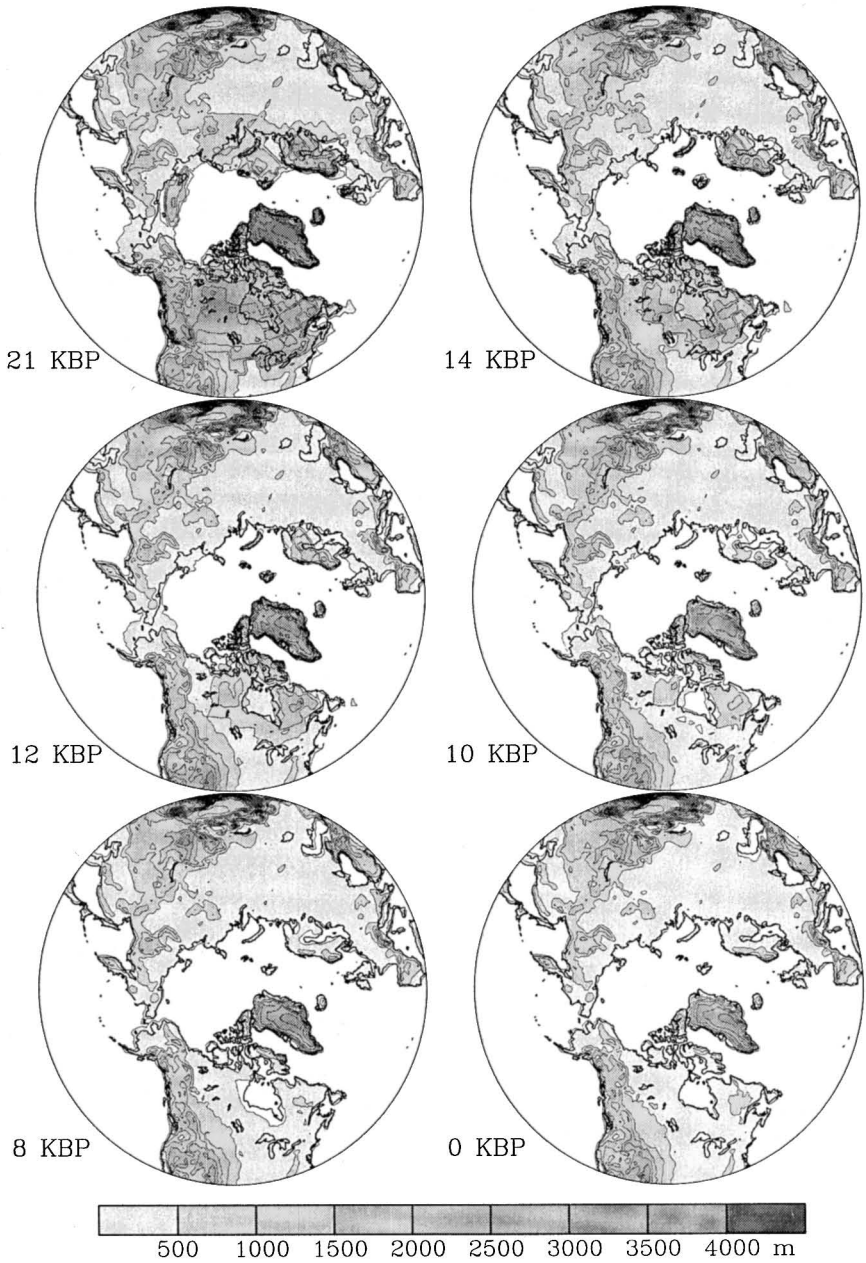

Fig. 16. Topography with respect to mean sea level isopachs for the Northern hemisphere component of ICE-4G for six times from Last Glacial Maximum to the present day. Note in particular the sharp declines in topography that occur with time over the Hudson Bay, the Gulf of Bothnia and the Barents and Kara Seas.

in which C is the surface heat capacity which is space dependent so as to distinguish land from sea and land ice and sea ice, T is the absolute temperature, Q is the solar constant (1360 Wm^{-2}), a ($\underline{r}$, t) is the surface albedo, S′(θ, t) is the solar distribution function through which orbital insolation anomalies may be introduced and NAHF ($\underline{r}$, t) is a contribution to atmospheric heating "from below" due to time dependence of the thermohaline circulation (restricted to the North Atlantic). The expression A+BT is an empirical representation of the infrared emission of radiation to space in which the parameter values A and B are obtained by fitting to satellite observations while the final term is a diffusive approximation to the redistribution of heat that occurs due to atmospheric dynamical processes. In the latter term the diffusion coefficient D is expressed by a low order expansion in Legendre polynomials that is constrained so as to allow the model to fit the modern latitudinal variation of surface temperature.

The energy balance atmosphere (23) is coupled to a model of ice sheet accumulation and flow that also takes the form of a nonlinear diffusion equation, viz:

$$\frac{\partial H}{\partial t} = \underline{\nabla}_h \left[B(\rho_I g)^m H^{m+1} \left(\underline{\nabla}_h h \cdot \underline{\nabla}_h h \right)^{\frac{m-1}{2}} \underline{\nabla} h \right] + G(\underline{r}, t) \tag{24}$$

in which H is ice thickness, h is ice sheet height above sea level, B (= 9.0 $m^{-3/2}$ yr^{-1}) is an empirical constant selected to enable the model to match observed ice-sheet aspect ratios and G ($\underline{r}$, t) is the so-called mass-balance function which determines the net accumulation at each point on the surface of the ice-sheet. In general, continental ice sheets are such that the net mass balance is positive over the central portion of the sheet where precipitation falls as snow that is converted into ice by compaction, whereas it is negative near the edge(s) where ablation is dominant. This ice-dynamics component of the model is linked to the energy balance model by the GIA process which, for climatological purposes, may often be represented as a simple local damped return to equilibrium as:

$$\frac{dh}{dt} = \frac{-h - h_o}{\tau} + \frac{\rho_I}{\rho_E} \frac{H}{\tau} \tag{25}$$

with τ a single characteristic relaxation time for the process, the data shown on Figure 6 suggesting that the choice $\tau \simeq$ 5-6 kyr would be most reasonable. The reason why the GIA process may exert strong feedback upon climate system behaviour is that the surface mass balance G($\underline{r}$, t) is strongly temperature dependent.

Imagine a situation such that the Laurentide ice-sheet is being driven to retreat subsequent to LGM by the Milankovitch variations in insolation. It is pinned to the North by the low temperatures that obtain in the Arctic and retreats by a northward migration of its southern periphery. As the ice margin moves northwards it does so into the deep depression created by the GIA process. However, because of the steep (negative) vertical gradient of atmospheric temperature, the temperature in the lowermost regions of the ablation zone rises rapidly causing the ablation rate to increase markedly. This constitutes a positive feedback on the retreat process and

thus accelerates the process of deglaciation. That this feedback is quite plausibly the main determinant of the rapid terminations that mark the completion of each 100 kyr cycle of glaciation and deglaciation will be clear on the basis of Figure 17 where I show the cycle of glaciation and deglaciation predicted by this model beginning from the last (Eemean) interglacial when the model is forced by the Milankovitch variations of insolation (e.g. [65]) that subsequently occurred. The global history of ice volume variations is compared in plate (a) with both the SPECMAP $\delta^{18}0$ proxy for global ice volume of [62] and with the time series for Northern Hemisphere insolation at 65°N latitude. The predicted ice volume variation is labelled Wbase in the Figure and this is assumed to include the component from Antarctica that is indicated. Clearly the theory very nicely fits the SPECMAP $\delta^{18}0$ data; especially important in this regard is the excellent fit that the model achieves to the fast "termination". In plate (b) of Figure 17 is shown a further series of synthetic ice volume predictions produced using variations on the basic analysis procedure employed to deliver the standard case result called Wbase in plate (a). The result called "non-perturbative" was obtained by using the energy balance component of the model to predict absolute ground temperature itself rather than the perturbation away from the modern "reanalysis" climatology data set as was done to obtain Wbase. In non-perturbative mode the model clearly predicts that no significant surface glaciation occurs prior to about 80,000 years before present, a result that is discordant with the observational evidence (e.g. the SPECMAP $\delta^{18}0$ record). Also shown in plate (b) is the time series labelled "non-perturb., old" which is that obtained in [66] with the version of the model that was further developed in [36] to obtain the results being described herein. With this version of the model no complete "termination" of the glacial cycle was predicted at all. In order to properly capture this dominant feature of the ice-age cycle, all of the improvements to the model discussed in the recent paper by Tarasov and Peltier [36] were required. This is the first model that has been successful in predicting the 100 kyr cycle that has not had to rely upon the ad hoc introduction of poorly constrained and highly questionable additional feedback mechanisms.

Of utmost interest for the purpose of the present paper, however, is the degree to which this successful model of the 100 kyr cycle relies upon the positive feedback associated with the GIA process to effect "termination" of the glacial epoch. This is examined in Figure 18 where, in the upper and lower plates respectively, the synthetic ice volume histories for North America and Northwestern Europe are shown separately and as a function of the model of mantle rheology used to describe the GIA process. On this Figure results are shown for several different versions of the "local-relaxation-to-equilibrium" model embodied in equation (22) which differ from one another only in the single relaxation time selected to describe the process. The choice $\tau = 1$ Myr clearly leads to a model which contains no isostatic adjustment at all and inspection of the time series for the North American ice-sheet delivered by the model in this case shows that in the absence of GIA related feedback the fast termination of the glacial epoch is essentially eliminated. Furthermore, complete termination is only realized with $\tau \simeq 5$ kyr, precisely the range of relaxation times required to understand the rsl data shown on Figure 6 from sites in the Hudson Bay region. Also shown on this Figure, as well as in plate (b), are results for the complete Maxwell linear viscoelastic model and this is also seen to deliver an acceptable facsimile of the termination of North American glaciation. Plate (b) shows a similar sequence of analyses for the Northwestern European ice volume time series. For this smaller scale ice-sheet GIA feedback appears not to play

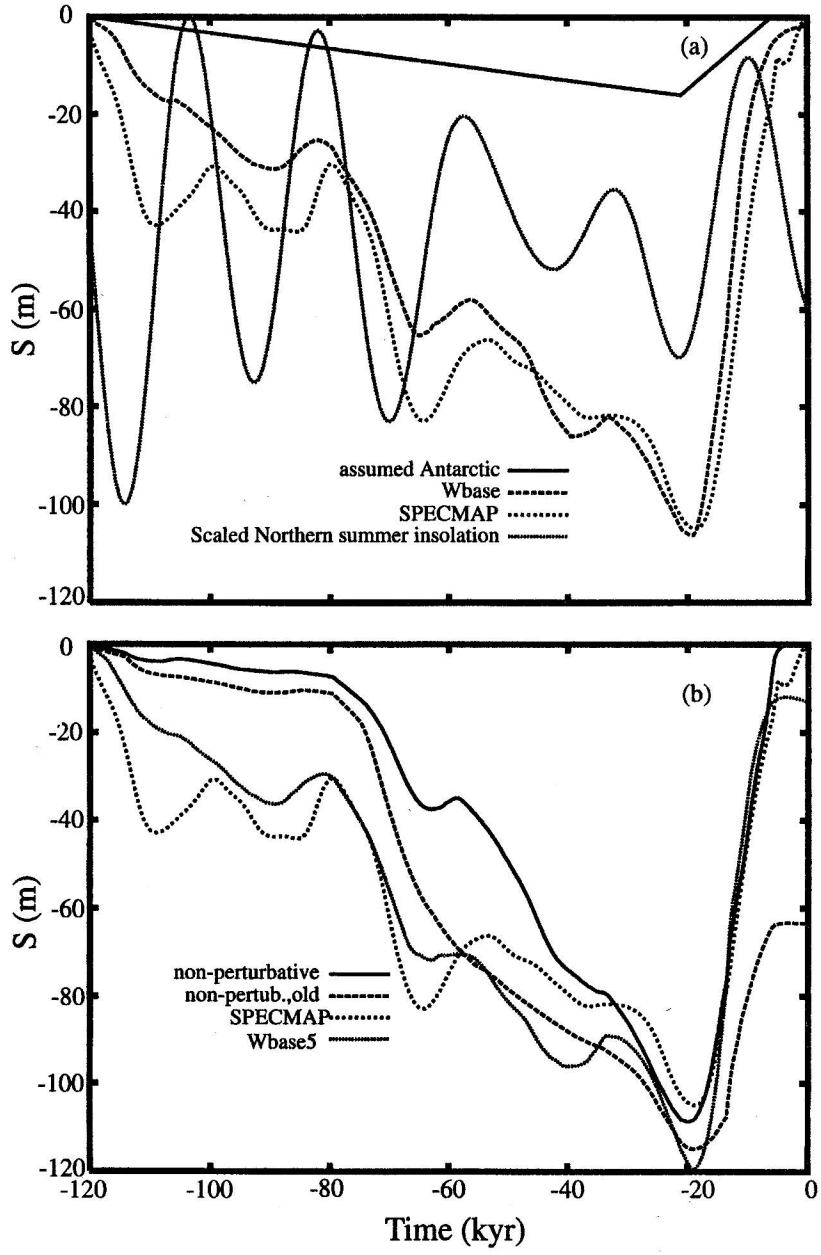

Fig. 17. Model predicted histories of eustatic sea level change over the last ice cycle. (a) These histories include an assumed Antarctic contribution of 16 m at -21 kyr. The curve labelled SPECMAP is the SPECMAP $\delta^{18}0$ time series [62] scaled to a particular LGM ice volume. Wbase is the time series predicted by the control model with 0.5 degree spatial resolution and an assumed temperature lapse rate of 7.5°K km^{-1}. Also shown for reference is a summertime seasonal - Cont.

the same significant role that it does for the dominant Laurentide ice mass. Complete termination is much less strongly dependent upon this influence.

5. Conclusions

In the foregoing sections of this paper I have reviewed, and commented upon, selected aspects of the global theory of the glacial isostatic adjustment that my students and I at Toronto have continued to develop over the last two decades. The most important recent advances that have been achieved in this work relate to (1) the extension of the Sea Level Equation formalism to allow accurate incorporation of time dependence of the ocean function as well as the (much less important) feedback associated with changing rotation, and (2) the development of a formal methodology with which the depth dependence of mantle viscosity may be inferred on the basis of an appropriate mix of GIA related observations. Also of considerable interest, I believe, are the insights that this theoretical work has begun to provide on a range of issues in climate dynamics, including the physics of the 100 kyr ice-age cycle itself, as discussed in the last Section. A far more detailed recent review of these ideas than I am able to provide here will be found in [37]. In a further contribution to this volume, I address the question of the constraints on the present day rate of global sea level rise that may be obtained on the basis of analyses with this global theory of the GIA process.

Fig. 17 continued. insolation time series (July at 65°N latitude) rescaled to sea level. (b) Wbase5 is as Wbase except for a modification of the PPD scheme used to compute ablation (see [36] for details). The curve denoted "non-perturbative" uses updated mass-balance parameterizations, input topography and input precipitation fields, but it does not correct the EBM output with reanalysis climatology. The curve labelled "non-perturbative, old", is the result obtained in [66] with 1° resolution, reduced precipitation and reduced flow parameter and which fails to deliver the observed termination. See [36] for details.

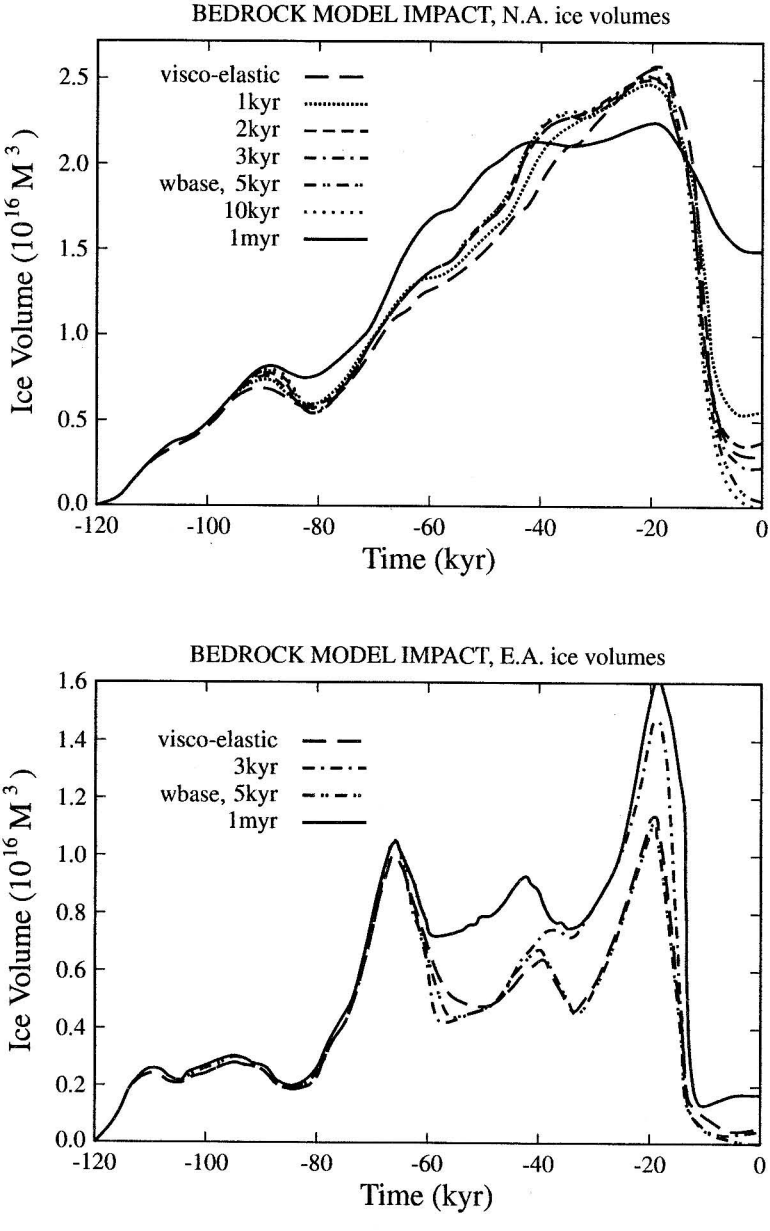

Fig. 18. Model predicted ice volume time series from Eeamen to present as a function of the way in which the GIA process is treated in the climate model. When the relaxation time employed in the context of the locally damped return to equilibrium model is made, so large that no subsidence under the ice sheets occurs, then the model fails to predict the termination.

References

[1] W.R. Peltier, *Rev. Geophys. Space Physics*, 12(1974), p. 649.
[2] W.E. Farrell, *Rev. Geophys. Space Phys.*, 10(1972), p. 761.
[3] M.A. Biot, *J. Appl. Phys.*, 25 (1954), p. 1385.
[4] W.R. Peltier, *Geophys. J.R. Astron. Soc.*, 46(1976), p. 669.
[5] A.E.S. Love, Some Problems of Geodynamics. Cambridge University Press(1911). Reprinted by Dover Publications Inc., 1967.
[6] W.R. Peltier, W.R., *J. Geophys. Res.*, 90(1985), p. 9411.
[7] P. Wu, The Response of a Maxwell Earth to Applied Surface Mass Loads: Glacial Isostatic Adjustment, M.Sc. Thesis, Department of Physics, University of Toronto(1978).
[8] M. Fang and B.H. Hager, *Geophys. J. Int.*, 123(1995), p. 849.
[9] W.R. Peltier, *Geophys. Res. Lett.*, 22(1995), p. 465.
[10] W.R. Peltier, *Geophys. J.R. Astron. Soc.*, 46(1976), p. 669.
[11] G.W. Platzman, In Mathematical Problems in the Geophysical Sciences 2. Inverse Problems, Dynamo Theory and Tides, W.H. Reid Ed., p. 239, Lectures in Applied Mathematics, Volume 14(1971). Am. Math. Sco., Providence, Rhode Island.
[12] W.E. Farrell and J.A. Clark, *Geophys. J.R. astr. Soc.*, 46(1976), p. 647.
[13] W.R. Peltier and J.T. Andrews, *Geophys. J.R. Astron. Soc.*, 46(1976), p. 605.
[14] J.A. Clark, W.E. Farrell and W.R. Peltier, *Quat. Res.*, 9(1978), p. 265.
[15] W.R. Peltier, W.E. Farrell and J.A. Clark, *Tectonophysics,* 50(1978), p. 81.
[16] P. Wu and W.R. Peltier, *Geophys. J.R. astr. Soc.*, 74(1983), p. 377.
[17] J.X. Mitrovica and W.R. Peltier, *J. Geophys. Res.*, 94(1989), p. 13651.
[18] W.R. Peltier, A.M. Forte, J.X. Mitrovica and A.M. Dziewonski, *Geophys. Res. Lett.*, 19(1992), p. 1555.
[19] G. Pari and W.R. Peltier, *J. Geophys. Res.*, 101(1996), p. 28105.
[20] S.R. Dickman, *Geophys. J. Roy. Astron. Soc.*, 57(1977), p. 41.
[21] R. Sabadini and W.R. Peltier, *Geophys. J.R. astr. Soc.*, 66(1981), p. 553.
[22] W.R. Peltier, *Advances in Geophysics*, 24(1982), p. 1.
[23] P. Wu and W.R. Peltier, *Geophys. J.R. astr. Soc.*, 76(1982), p. 202.
[24] C.F. Yoder, J.G. Williams, J.O. Dickey, B.E. Schutz, R.J. Eanes and B.D. Tapley, *Nature*, 303(1983), p. 757.
[25] W.R. Peltier, *Nature*, 304(1983), p. 434.
[26] D.F. Argus, *Geophys. Res. Lett.*, 23(1996), p. 973.
[27] W.R. Peltier, *Science*, 265(1994), p. 195.
[28] W.R. Peltier, *Science*, 267(1995), p. 536.
[29] BIFROST Project, *EOS, Transactions, American Geophysical Union*, Volume 77(1996), August 27.
[30] T.S. James and A. Lambert, *Geophys. Res. Lett.*, 20(1993), p. 870.
[31] J.X. Mitrovica, J.L. Davis and I.I. Shapiro, *J. Geophys. Res.*, 99(1994), p. 7075.
[32] W.R. Peltier, *Geophys. Res. Lett.*, (1998) in press.
[33] W.R. Peltier, *Science*, 273(1996), p. 1359.
[34] G. Vettoretti, W.R. Peltier and N.A. McFarlane, *Journal of Climate*, (1998) in press.
[35] L. Tarasov, and W.R. Peltier, *Ann. of Glaciol.*, (1998) in press.

[36] L. Tarasov and W.R. Peltier, *J. Geophys. Res.-Atmospheres*, 102(1997), p. 21665.
[37] W.R. Peltier, *Rev. Geophys.*, (1998) in press.
[38] W.R. Peltier and A.M. Tushingham, *Science*, 244(1989), p. 806.
[39] W.R. Peltier, *Geophys. Res. Lett.*, 23(1996), p. 717.
[40] W.R. Peltier and Xianhua Jiang, *Surveys in Geophysics*, 18(1997), p. 239.
[41] W.R. Peltier, Global Planetary Change, (1998) in press.
[42] W.R. Peltier, Inverse Problems, (1998) in press.
[43] W.R. Peltier and X. Jiang, *J. Geophys. Res.*, 101(1996), p. 3269.
[44] W.R. Peltier, *J. Geophys. Res.*, 102(1997), p. 10101.
[45] W.H. Munk and G.F. MacDonald, G.F., The Rotation of the Earth, Cambridge Univ. Press, London and New York (1960).
[46] F.A. Dahlen, *Geophys. J.R. astr. Soc.*, 46(1976), p. 363.
[47] B.G. Bills, and Thomas S. James, *Geophys. Res. Lett.*, 23(1996), p. 3023.
[48] W.R. Peltier, in A. Dziewonski and E. Boschi eds. Physics of the Earth's Interior, Proceedings of the Enrico Fermi Summer School in Physics, North Holland Publishing Company, pp. 362-431 (1980).
[49] W.R. Peltier and X. Jiang, *Geophys. Res. Lett.*, 23(1996), p. 503.
[50] A. Tarantola and B. Valette, *J. Geophys.*, 50(1982), p. 159.
[51] A. Tarantola and B. Valette, *Rev. Geophys. Space Phys.*, 20(1982), p. 219.
[52] D.D. Jackson and J. Matsu'ura, *J. Geophys. Res.*, 90(1985), p. 581.
[53] G.E. Backus, *Geophys. J.R. astr. Soc.*, 92(1988), p. 125.
[54] A.M. Tushingham and W.R. Peltier, *J. Geophys. Res.*, 97(1992), p. 3285.
[55] R.K. McConnell, *J. Geophys. Res.*, 73(1968), p. 7089.
[56] A.M. Forte, A.M. Dziewonski and R.L. Woodward, In Dynamics of the Earth's Deep Interior and Earth Rotation, (Geophys. Monogr. Ser.), Vol. 72, edited by J.-L. Le Mouel, pp. 135-166, AGU, Washington, D.C. (1993).
[57] G. Pari and W.R. Peltier, *J. Geophys. Res.*, 100(1995), p. 12731.
[58] G. Pari W.R. Peltier, *J. Geophys. Res.*, (1998) submitted.
[59] P. Wu and W.R. Peltier, *Geophys. J.R. astr. Soc.*, 70(1982), p. 435.
[60] A.M. Forte and W.R. Peltier, *Advances in Geophysics*, 36(1994), p. 1.
[61] D.F. Argus and W.R. Peltier, *J. Geophys. Res.*, (1996) submitted.
[62] J. Imbrie, J.D. Hays, D.G. Martinsen, A. McIntyre, A.C. Mix, J.J. Morley, N.G. Pisias, W.L. Prell and N.J. Shackleton, In Milankovitch and Climate (A Berger et al. eds.), pp. 269-306. Reidell Publ. Boston, Massachusetts (1984).
[63] R.G. Fairbanks, *Nature*, 342(1989), p. 637.
[64] E. Bard, B. Hamelin, R.G. Fairbanks and A. Zindler, *Nature*, 345(1990), p. 405
[65] A. Berger, *J. Atmos. Sci.*, 35(1978), p. 2362.
[66] W.R. Peltier and S. Marshall, *J. Geophys. Res.*, 100(1995), p. 14269.